ASC Report No. 01/2007

Simple A Posteriori Error Estimators for the h-Version of the Boundary Element Method

Samuel Ferraz-Leite, Dirk Praetorius

Institute for Analysis and Scientific Computing
Vienna University of Technology — TU Wien
www.asc.tuwien.ac.at ISBN 978-3-902627-00-1

Institute for Analysis and Scientific Computing
Vienna University of Technology
Wiedner Hauptstraße 8–10
1040 Wien, Austria

E-Mail: admin@asc.tuwien.ac.at
WWW: http://www.asc.tuwien.ac.at
FAX: +43-1-58801-10196

ISBN 978-3-902627-00-1

ASC
TU WIEN

SIMPLE A POSTERIORI ERROR ESTIMATORS FOR THE h-VERSION OF THE BOUNDARY ELEMENT METHOD

SAMUEL FERRAZ-LEITE AND DIRK PRAETORIUS

ABSTRACT. The h-$h/2$-strategy is one well-known technique for the a posteriori error estimation for Galerkin discretizations of energy minimization problems. One considers $\eta_H := \|\phi_h - \phi_{h/2}\|$ to estimate the error $\|\phi - \phi_h\|$, where ϕ_h is a Galerkin solution with respect to a mesh $\mathcal{T}_h$ and $\phi_{h/2}$ is a Galerkin solution with respect to the mesh $\mathcal{T}_{h/2}$ obtained from a uniform refinement of $\mathcal{T}_h$. This error estimator is always efficient and observed to be also reliable in practice. However, for boundary element methods, the energy norm is non-local and thus the error estimator η_H does not provide information for a local mesh-refinement. Recent localization techniques allow to replace the energy norm in this case by weighted L^2-norms resp. H^1-seminorms. Therefore, this very basic error estimation strategy is also applicable to steer an h-adaptive algorithm for the boundary element method. Numerical experiments in 2D and 3D show that the proposed method works well in practice. As model examples serve the elliptic first-kind integral equations with weakly singular and hypersingular integral kernel.

Dedicated to Professor Ernst P. Stephan on the occasion of his 60th birthday

1. Introduction and Model Example

We consider Symm's integral equation

$$V\phi = f \quad \text{on } \Gamma \tag{1.1}$$

for a relatively open subset $\Gamma \subseteq \partial\Omega$ of the boundary of a bounded Lipschitz domain $\Omega \subseteq \mathbb{R}^d$, for $d = 2, 3$. Here, $V\phi$ denotes the simple-layer potential

$$V\phi(x) = \int_\Gamma G(x-y)\phi(y)\, ds_y \quad \text{for } x \in \Gamma \tag{1.2}$$

with $G(\cdot)$ the fundamental solution of the Laplacian, i.e.

$$G(z) = \begin{cases} -\frac{1}{2\pi}\log|z| & \text{for } d = 2, \\ +\frac{1}{4\pi}|z|^{-1} & \text{for } d = 3, \end{cases} \tag{1.3}$$

and with $\int_\Gamma ds$ the integration over the surface piece Γ. The operator $V : \widetilde{H}^{-1/2}(\Gamma) \to H^{1/2}(\Gamma)$ is an elliptic isomorphism between the fractional-order Sobolev space $\mathcal{H} := \widetilde{H}^{-1/2}(\Gamma)$ and its dual $\mathcal{H}^* = H^{1/2}(\Gamma)$, where we additionally assume $\operatorname{diam}(\Omega) < 1$ in case of $d = 2$. It thus provides an equivalent scalar product $\langle\!\langle \cdot, \cdot \rangle\!\rangle$ on the energy space $\mathcal{H}$ defined by $\langle\!\langle \phi, \psi \rangle\!\rangle :=$

Date: July 27, 2007.

1991 *Mathematics Subject Classification.* 65N38,65R20,65N50.

Key words and phrases. Symm's integral equation, hypersingular integral equation, boundary element method, Galerkin method, a posteriori error estimate, adaptive algorithm.

$\langle V\phi, \psi\rangle$. Here, the duality brackets $\langle\cdot,\cdot\rangle$ extend the $L^2(\Gamma)$-scalar product. We denote by $|||\cdot|||$ the induced energy norm.

Given $f \in \mathcal{H}^*$, the unique solution $\phi \in \mathcal{H}$ of (1.1) solves

$$\langle\!\langle \phi, \psi \rangle\!\rangle = \langle f, \psi\rangle \quad \text{for all } \psi \in \mathcal{H}. \tag{1.4}$$

Let $\mathcal{T}_h$ be a triangulation of Γ (with local mesh-size h). Then, the lowest-order Galerkin method is to find a $\mathcal{T}_h$-piecewise constant function $\phi_h \in \mathcal{P}^0(\mathcal{T}_h)$ which solves

$$\langle\!\langle \phi_h, \psi_h \rangle\!\rangle = \langle f, \psi_h\rangle \quad \text{for all } \psi_h \in \mathcal{P}^0(\mathcal{T}_h). \tag{1.5}$$

We stress the Galerkin orthogonality

$$\langle\!\langle \phi - \phi_h, \psi_h \rangle\!\rangle = 0 \quad \text{for all } \psi_h \in \mathcal{P}^0(\mathcal{T}_h), \tag{1.6}$$

which in fact characterizes the discrete solution ϕ_h. The goal of this work is to contribute to the simple and accurate a posteriori estimation for the error $|||\phi - \phi_h|||$ in the energy norm: An a posteriori error estimator is a computable quantity η which does not depend on the (in general unknown) exact solution ϕ but on a computed discrete solution ϕ_h and which estimates the error $|||\phi - \phi_h|||$ in the energy norm. We aim to provide estimates

$$C_{\rm eff}^{-1}\,\eta \le |||\phi - \phi_h||| \le C_{\rm rel}\,\eta \tag{1.7}$$

which are referred to as efficiency (lower estimate) and reliability (upper estimate) of η, respectively. The constants $C_{\rm eff}, C_{\rm rel}$ may not depend on ϕ or ϕ_h, but on the given right-hand side $f \in \mathcal{H}^*$ as well as weakly on $\mathcal{T}_h$, e.g., on the shape of the elements in $\mathcal{T}_h$.

To introduce the analytical idea of this paper, let $\mathcal{T}_{h/2}$ be a second triangulation of Γ obtained from a uniform refinement of $\mathcal{T}_h$. We consider the discrete spaces $X_h := \mathcal{P}^0(\mathcal{T}_h)$ and $X_{h/2} := \mathcal{P}^0(\mathcal{T}_{h/2})$ with corresponding Galerkin solutions $\phi_h \in X_h$ and $\phi_{h/2} \in X_{h/2}$, respectively. Recall that the best approximation property of the Galerkin solution with respect to the energy norm and $X_h \subset X_{h/2}$ provides

$$|||\phi - \phi_{h/2}||| \le |||\phi - \phi_h|||. \tag{1.8}$$

In a first step, we now consider the h-$h/2$-error estimator

$$\eta_H := |||\phi_h - \phi_{h/2}|||. \tag{1.9}$$

The Galerkin orthogonality (1.6) for $\mathcal{P}^0(\mathcal{T}_{h/2})$ yields

$$|||\phi - \phi_h|||^2 = |||\phi - \phi_{h/2}|||^2 + |||\phi_{h/2} - \phi_h|||^2 = |||\phi - \phi_{h/2}|||^2 + \eta_H^2$$

and thus $\eta_H \le |||\phi - \phi_h|||$. This proves efficiency of η_H with $C_{\rm eff} = 1$. The reliability of η_H is usually proven with the help of the **saturation assumption**, which is a strengthened version of (1.8) and reads

$$|||\phi - \phi_{h/2}||| \le q\,|||\phi - \phi_h||| \tag{A}$$

with a uniform constant $q \in (0,1)$. Under this assumption, we obtain $|||\phi - \phi_h|||^2 = |||\phi - \phi_{h/2}|||^2 + \eta_H^2 \le q^2\,|||\phi - \phi_h|||^2 + \eta_H^2$ and thus reliability

$$|||\phi - \phi_h||| \le \frac{1}{\sqrt{1-q^2}}\,\eta_H. \tag{1.10}$$

We state these observations in the following proposition for later reference. We stress that our considerations are, so far, independent of the precise mathematical setting, e.g., Symm's integral equation.

Proposition 1.1. (i) *The h-h/2-error estimator η_H is always efficient with $C_{\rm eff} = 1$.*
(ii) *Under the saturation assumption* (A)*, η_H is reliable with $C_{\rm rel} = 1/\sqrt{1-q^2}$.* □

For the finite element method, the saturation assumption (A) can be proven under some mild conditions on the local mesh refinement, c.f. [D, DN]. However, we stress that the saturation assumption — although observed in praxis — has not been proven for the boundary element method, yet.

An additional difficulty for boundary element methods is the non-locality of the energy norm, e.g. $|||\cdot||| \sim \|\cdot\|_{\widetilde{H}^{-1/2}(\Gamma)}$ for Symm's integral equation. Here, non-locality of the norm means that $|||\cdot|||$ cannot be written as sum of local contributions — in contrast to, e.g., the L^2-norm which satisfies $\|\cdot\|^2_{L^2(\Gamma)} = \sum_{T\in\mathcal{T}_h} \|\cdot\|^2_{L^2(T)}$. One therefore needs so-called localization techniques which provide lower and upper estimates for $|||\phi_h - \phi_{h/2}|||$ by use of, e.g., weighted L^2-norms. We use recent ideas from [CP2] to prove that, for shape-regular meshes,

$$\mu_H = \|h^{1/2}(\phi_h - \phi_{h/2})\|_{L^2(\Gamma)} \tag{1.11}$$

is an equivalent error estimator, i.e. there are constants $C_1, C_2 > 0$ such that

$$C_1^{-1}\mu_H \le \eta_H \le C_2\mu_H. \tag{1.12}$$

Here $h \in L^\infty(\Gamma)$, $h|_T := \operatorname{diam}(T)$ for $T \in \mathcal{T}_h$, denotes the local mesh-size function. For our numerical experiments, we thus may use the local contributions $\mu_{H,j} := \operatorname{diam}(T_j)^{1/2}\|\phi_h - \phi_{h/2}\|_{L^2(T_j)}$ to decide whether an element $T_j \in \mathcal{T}_h$ should be refined or not.

The content of this paper is organized as follows: In Section 2 we recall some notations and restrictions for the triangulations under consideration. In Section 3, we provide the localization of the energy norm in case of Symm's integral equation. The analogous results for the hypersingular integral equation are proven in Section 4. In Section 5, we apply the localization techniques to the boundary integral formulation of a transmission problem. Numerical experiments in 2D and 3D are found in Section 6 and 7. We stress that our analysis, so far, is restricted to the case of isotropic mesh-refinement in 3D. However, the concluding numerical experiments in Section 8 underline that the developed techniques are capable to control the discretization error even in case of anisotropic mesh-refinement. Some concluding remarks are drawn in Section 9.

2. Preliminaries

General Triangulations and Piecewise Polynomials. Let $\mathcal{T}_h = \{T_1, \dots, T_N\}$ be a triangulation of Γ, i.e.

- $\overline{\Gamma} = \bigcup_{j=1}^N T_j$, i.e. $\mathcal{T}_h$ covers $\overline{\Gamma}$,
- each $T_j \in \mathcal{T}_h$ is closed and non-degenerate, i.e. $|T_j| > 0$,
- $|T_j \cap T_k| = 0$ for the intersection of two elements $T_j, T_k \in \mathcal{T}_h$ with $T_j \neq T_k$.

Here, $|\cdot|$ denotes the $(d-1)$-dimensional surface measure. For the ease of presentation, we assume that, for $d = 2$, the elements $T_j \in \mathcal{T}_h$ are affine boundary pieces. For $d = 3$, the elements $T_j \in \mathcal{T}_h$ are assumed to be either flat triangles or flat rectangles, respectively. For $p \ge 0$, we denote by $\mathcal{P}^p(\mathcal{T}_h)$ the space of all $\mathcal{T}_h$-piecewise polynomials. As usual, these

discrete functions are defined on a reference element $T^{\rm ref}$ and mapped onto the respective elements by affine transformations. The reference element is given by $T^{\rm ref}_{2D} = [0,1]$ in case of $d=2$, and either $T^{\rm ref}_{3D,\triangle} = {\rm conv}\{(0,0),(0,1),(0,1)\}$ or $T^{\rm ref}_{3D,\square} = [0,1]^2$ in case of $d=3$.

Local Mesh-Widths and K-Mesh Property. For each element $T_j \in \mathcal{T}_h$, we define the diameter $h_j := {\rm diam}(T_j) > 0$. Moreover, let $\varrho_j > 0$ be the diameter of the largest sphere centred at a point in T_j, whose intersection with Γ lies entirely inside T_j. To deal with error estimates on adaptively refined meshes, we define local mesh-width functions $h, \varrho \in L^\infty(\Gamma)$ by $h|_{T_j} := h_j$ and $\varrho|_{T_j} := \varrho_j$ for $T_j \in \mathcal{T}_h$, respectively. Obviously, there holds $\varrho = h$ pointwise for $d=2$, whereas only $\varrho \le h$ for $d=3$. We thus define the shape-regularity constant

$$\sigma(\mathcal{T}_h) := \sup_{T_j \in \mathcal{T}_h} (h_j/\varrho_j) = \|h/\varrho\|_{L^\infty(\Gamma)} \ge 1. \tag{2.1}$$

By definition, there holds the pointwise estimate $\varrho \le h \le \sigma(\mathcal{T}_h)\varrho$, where $\sigma(\mathcal{T}_h) = 1$ for $d=2$.

A mesh-refinement strategy, which yields a sequence $(\mathcal{T}_h^{(\ell)})$ of triangulations, is called *isotropic*, provided that $\sigma_0 := \sup_{\ell\in\mathbb{N}} \sigma(\mathcal{T}_h^{(\ell)}) < \infty$. However, the mesh-refinement strategies of practical interest often lead to an anisotropic mesh-refinement. More precisely, the adaptive meshes obtained below satisfy the K-mesh property for some constant $\kappa(\mathcal{T}_h) \ge 1$, i.e. there hold:

- For any $T_j, T_k \in \mathcal{T}_h$ with $T_j \cap T_k \neq \emptyset$ holds $h_j/h_k \le \kappa(\mathcal{T}_h)$ as well as $\varrho_j/\varrho_k \le \kappa(\mathcal{T}_h)$, i.e. the local mesh-widths of neighbouring elements do not vary too rapidly.
- For any node $z \in \overline{\Gamma}$ of $\mathcal{T}_h$ holds $\#\{T \in \mathcal{T}_h : z \in T\} \le \kappa(\mathcal{T}_h)$, i.e. each node does not belong to too many elements of $\mathcal{T}_h$.

We stress that the estimates below depend on (an upper bound of) the mesh-constant $\kappa(\mathcal{T}_h)$.

Regular Meshes vs. Hanging Nodes. We recall that the triangulation $\mathcal{T}_h$ is *regular* in the sense of Ciarlet, if, for all elements $T_j, T_k \in \mathcal{T}_h$ with $T_j \neq T_k$, the intersection $T_j \cap T_k$

- is either empty,
- or a vertex of both T_j and T_k,
- or an edge of both T_j and T_k.

These properties are needed to ensure global continuity and thus H^1-conformity of certain $\mathcal{T}_h$-piecewise polynomials.

However, for the analysis of Symm's integral equation we may deal with discontinuous $\mathcal{T}_h$-piecewise polynomials to discretize the energy space $\widetilde{H}^{-1/2}(\Gamma)$. In this case, we thus drop the regularity assumption and allow hanging nodes instead. For the analysis, we shall assume that $\mathcal{T}_h$ is *almost regular*, i.e. there is a regular triangulation $\widehat{\mathcal{T}}_h$ of Γ such that

- $\widehat{\mathcal{T}}_h$ is obtained from certain refinements of $\mathcal{T}_h$, i.e. $\mathcal{P}^0(\mathcal{T}_h) \subseteq \mathcal{P}^0(\widehat{\mathcal{T}}_h)$,
- there is a constant $\widehat{\kappa}(\mathcal{T}_h)$, which only depends on $\mathcal{T}_h$ such that

$$\kappa(\widehat{\mathcal{T}}_h) \le \widehat{\kappa}(\mathcal{T}_h)\,\kappa(\mathcal{T}_h) \tag{2.2}$$

  and that

$$\widehat{h} \le h \le \widehat{\kappa}(\mathcal{T}_h)\,\widehat{h} \quad \text{as well as} \quad \widehat{\varrho} \le \varrho \le \widehat{\kappa}(\mathcal{T}_h)\,\varrho. \tag{2.3}$$

  Here, h and ϱ as well as $\widehat{h}$ and $\widehat{\varrho}$ denote the mesh-width functions with respect to $\mathcal{T}_h$ and $\widehat{\mathcal{T}}_h$, respectively.

We stress that both assumptions hold for the 3D experiments provided below.

3. Symm's Integral Equation

For the entire section, let $\mathcal{T}_h$ be an almost-regular triangulation of Γ. We adopt the notations of the introductory section. The first lemma provides a localization of the $\widetilde{H}^{-1/2}$-norm for discrete functions $v_h \in L^2(\Gamma)$. This localization is naturally given in terms of a mesh-size weighted L^2-norm. The inverse estimate (3.1) is proven in [GHS]. The approximation estimates (3.2)–(3.3) are taken from [CP2].

Lemma 3.1. (i) *For any discrete function $v_h \in \mathcal{P}^0(\mathcal{T}_h)$ holds the inverse estimate*

$$\|\varrho^{1/2} v_h\|_{L^2(\Gamma)} \leq C_3 |\!|\!| v_h |\!|\!|, \tag{3.1}$$

where the constant $C_3 > 0$ only depends on Γ and the mesh-constants $\kappa(\mathcal{T}_h)$ and $\widehat{\kappa}(\mathcal{T}_h)$.
(ii) *For Π_h the L^2-projection onto $\mathcal{P}^0(\mathcal{T}_h)$ and any $v \in L^2(\Gamma)$ holds*

$$|\!|\!| v - \Pi_h v |\!|\!| \leq C_4 \|h^{1/2}(v - \Pi_h v)\|_{L^2(\Gamma)} \leq C_4 \|h^{1/2} v\|_{L^2(\Gamma)}. \tag{3.2}$$

The constant $C_4 > 0$ only depends on Γ but not on the triangulation $\mathcal{T}_h$.
(iii) *For $\mathbb{G}_h$ the Galerkin projection onto $\mathcal{P}^0(\mathcal{T}_h)$ and any $v \in L^2(\Gamma)$ holds*

$$|\!|\!| v - \mathbb{G}_h v |\!|\!| \leq C_4 \min\big\{ \|h^{1/2}(v - \mathbb{G}_h v)\|_{L^2(\Gamma)}, \|h^{1/2} v\|_{L^2(\Gamma)} \big\}. \tag{3.3}$$

(iv) *Neither of the constants C_3 and C_4 depend on the local mesh-sizes h and ϱ or on the number $\#\mathcal{T}_h$ of elements.* □

Sketch of Proof. Let $\widehat{\mathcal{T}}_h$ be the regular triangulation corresponding to $\mathcal{T}_h$ in the sense of the preliminary section. According to [GHS, Proposition 2.9], there holds

$$\|\varrho^{1/2} v_h\|_{L^2(\Gamma)} \leq C_3 |\!|\!| v_h |\!|\!| \quad \text{for all } v_h \in \mathcal{P}^0(\widehat{\mathcal{T}}_h),$$

where the constant $C_3 > 0$ depends only on $\kappa(\widehat{\mathcal{T}}_h)$ and thus on $\kappa(\mathcal{T}_h)$ and $\widehat{\kappa}(\mathcal{T}_h)$. In particular, (i) follows from $\mathcal{P}^0(\mathcal{T}_h) \subseteq \mathcal{P}^0(\widehat{\mathcal{T}}_h)$. (ii) is proven in [CP2, Theorem 4.1]. Therefore, the best approximation property of the Galerkin projection yields, for $v \in L^2(\Gamma)$,

$$|\!|\!| v - \mathbb{G}_h v |\!|\!| \leq |\!|\!| v - \Pi_h v |\!|\!| \leq C_4 \|h^{1/2} v\|_{L^2(\Gamma)}.$$

Defining, $w := v - \mathbb{G}_h v \in L^2(\Gamma)$ and observing $w - \mathbb{G}_h w = v - \mathbb{G}_h v$, we additionally obtain

$$|\!|\!| v - \mathbb{G}_h v |\!|\!| = |\!|\!| w - \mathbb{G}_h w |\!|\!| \leq C_4 \|h^{1/2} w\|_{L^2(\Gamma)} = C_4 \|h^{1/2}(v - \mathbb{G}_h v)\|_{L^2(\Gamma)}$$

The combination of the latter estimates proves (iii). □

***Remark* 1.** For the ease of presentation, we restrict to the lowest-order case. We stress that (3.2) holds under some richness assumptions on the discrete space X_h. Namely, we have to assume that $\Pi_h : L^2(\Gamma) \to X_h$ is the L^2-projection and that X_h contains at least either $P^0(\mathcal{T}_h)$ or $\mathcal{P}^1(\mathcal{T}_h) \cap C(\Gamma)$, where only in the latter case C_4 depends on the shape-regularity constant $\sigma(\mathcal{T}_h)$, c.f. [CP2]. The lower localization estimate holds for any $\widehat{\mathcal{T}}_h$-piecewise polynomial $v_h \in \mathcal{P}^p(\widehat{\mathcal{T}}_h)$, where the constant C_3 depends on the polynomial degree p and on the mesh-constant $\kappa(\widehat{\mathcal{T}}_h)$, c.f. [GHS]. The dependence of C_3 and C_4 on Γ follows from equivalence of norms $|\!|\!| \cdot |\!|\!| \sim \| \cdot \|_{\widetilde{H}^{-1/2}(\Gamma)}$. □

Theorem 3.2. *The a posteriori error estimator*

$$\mu_H := \|\varrho^{1/2}(\phi_h - \phi_{h/2})\|_{L^2(\Gamma)} \tag{3.4}$$

satisfies

$$(\sqrt{2}\,C_3)^{-1}\mu_H \le \eta_H \le C_4\,\sigma(\mathcal{T}_h)^{1/2}\,\mu_H \tag{3.5}$$

with the constants $C_3, C_4 > 0$ from Lemma 3.1. In particular, μ_H is always efficient.

Proof. Let $\mathbb{G}_h$ denote the Galerkin projection onto $\mathcal{P}^0(\mathcal{T}_h)$ and note that $\mathcal{P}^0(\mathcal{T}_h) \subset \mathcal{P}^0(\mathcal{T}_{h/2})$ implies $\mathbb{G}_h\phi_{h/2} = \phi_h$. Therefore, we have $\phi_h - \phi_{h/2} = (1-\mathbb{G}_h)(\phi_h - \phi_{h/2})$. Now, (3.3) proves

$$|||\phi_h - \phi_{h/2}||| = |||(1-\mathbb{G}_h)(\phi_h - \phi_{h/2})||| \le C_4\|h^{1/2}(\phi_h - \phi_{h/2})\|_{L^2(\Gamma)} \le C_4\|(h/\varrho)^{1/2}\|_{L^\infty(\Gamma)}\,\mu_H.$$

By definition, there holds $\sigma(\mathcal{T}_h)^{1/2} = \|(h/\varrho)^{1/2}\|_{L^\infty(\Gamma)}$, which leads to the upper estimate in (3.5). For the lower estimate, we use the inverse estimate (3.1) on $\mathcal{P}^0(\mathcal{T}_{h/2})$ to obtain

$$\|(\varrho/2)^{1/2}(\phi_h - \phi_{h/2})\|_{L^2(\Gamma)} \le C_3\,|||\phi_h - \phi_{h/2}|||,$$

which concludes the proof. □

***Remark* 2.** Theorem 3.2 states equivalence of η_H and μ_H in case of either $d = 2$ or isotropic mesh-refinement in case of $d = 3$. However, the numerical experiments below indicate that the critical estimate $\eta_H \lesssim \mu_H$ does even hold for anisotropic mesh-refinement. □

The following algorithm realizes an adaptive mesh-refining strategy based on the localized h-$h/2$-estimator μ_H.

Algorithm 3.3. *Let $\varepsilon > 0$ be a given tolerance and $\theta \in [0,1]$ the adaptivity parameter. Given $\ell := 0$ and an initial mesh $\mathcal{T}^{(0)}$, do the following:*

(i) *Refine $\mathcal{T}_h^{(\ell)}$ uniformly to obtain $\mathcal{T}_{h/2}^{(\ell)}$.*
(ii) *Compute Galerkin solutions $\phi_h^{(\ell)} \in \mathcal{P}^0(\mathcal{T}_h^{(\ell)})$ and $\phi_{h/2}^{(\ell)} \in \mathcal{P}^0(\mathcal{T}_{h/2}^{(\ell)})$.*
(iii) *Compute error estimator $\eta_H := |||\phi_h^{(\ell)} - \phi_{h/2}^{(\ell)}|||$ and stop provided $\eta_H \le \varepsilon$.*
(iv) *Compute refinement indicators $\mu_{H,j} := \varrho_j^{1/2}\|\phi_h^{(\ell)} - \phi_{h/2}^{(\ell)}\|_{L^2(T_j)}$ for $\mathcal{T}_h^{(\ell)} = \{T_1, \dots, T_N\}$.*
(v) *Mark $T_j \in \mathcal{T}_h^{(\ell)}$ for refinement provided $\mu_{H,j} \ge \theta \max\{\mu_{H,k} : k = 1, \dots, N\}$.*
(vi) *Refine the marked elements to obtain $\mathcal{T}_h^{(\ell+1)}$, update $\ell \mapsto \ell + 1$, and go to* (i). □

***Remark* 3.** We stress that we do some additional marking in (v) to guarantee that

$$\kappa(\mathcal{T}_h^{(\ell)}) \le C_5 \quad \text{as well as} \quad \widehat{\kappa}(\mathcal{T}_h^{(\ell)}) \le C_5$$

with a constant $C_5 > 0$ that only depends on $\mathcal{T}_h^{(0)}$ but not on ℓ. — For instance, in 2D, let T_j and T_k two neighbouring elements. If T_k is marked for refinement and $h_j > h_k$, we also mark T_j for refinement. By this procedure, we guarantee that $\kappa(\mathcal{T}_h^{(\ell)}) \le 2\,\kappa(\mathcal{T}_h^{(0)})$. □

***Remark* 4.** The choice of $\theta = 0$ leads to uniform mesh-refinement in Algorithm 3.3. For the numerical experiments below, we always used $\theta = 0.5$ for adaptive mesh-refinement. □

When Algorithm 3.3 stops with $\eta_H \le \varepsilon$, the Galerkin solution $\phi_{h/2}^{(\ell)}$ is a better approximation of ϕ than $\phi_h^{(\ell)}$ as $|||\phi - \phi_{h/2}^{(\ell)}||| \le |||\phi - \phi_h^{(\ell)}|||$. Thus, Algorithm 3.3 should usually return $\phi_{h/2}^{(\ell)}$ instead of $\phi_h^{(\ell)}$. From this point of view, the quantity ϕ_h becomes a temporary result only. One usually aims to compute side results with as less computational effort as possible. In our case, we can simply avoid to compute ϕ_h as follows:

Theorem 3.4. *With $\Pi_h : L^2(\Gamma) \to \mathcal{P}^0(\mathcal{T}_h)$ the L^2-projection, we define the error estimators*

$$\widetilde{\eta}_H := |||\phi_{h/2} - \Pi_h \phi_{h/2}||| \quad \text{and} \quad \widetilde{\mu}_H := \|\varrho^{1/2}(\phi_{h/2} - \Pi_h \phi_{h/2})\|_{L^2(\Gamma)}. \tag{3.6}$$

Then, there holds

$$\widetilde{\mu}_H \le \mu_H \le \sqrt{2}\, C_3\, \eta_H \quad \text{and} \quad \eta_H \le \widetilde{\eta}_H \le C_4\, \sigma(\mathcal{T}_h)^{1/2}\, \widetilde{\mu}_H \tag{3.7}$$

with the constants $C_3, C_4 > 0$ from Lemma 3.1. In particular, $\widetilde{\mu}_H$ is always efficient.

Proof. From the best approximation property of the Galerkin projection, we infer

$$\eta_H = |||\phi_{h/2} - \phi_h||| = |||(1 - \mathbb{G}_h)\phi_{h/2}||| \le |||(1 - \Pi_h)\phi_{h/2}||| = \widetilde{\eta}_H.$$

An application of (3.2) proves $\widetilde{\eta}_H \le C_4\, \|(h/\varrho)^{1/2}\|_{L^\infty(\Gamma)}\, \widetilde{\mu}_H$. To dominate $\widetilde{\mu}_H$ by μ_H, note that Π_h is the $\mathcal{T}_h$-elementwise L^2-projection, whence $\|(1 - \Pi_h)\phi_{h/2}\|_{L^2(T_j)} \le \|(1 - \mathbb{G}_h)\phi_{h/2}\|_{L^2(T_j)}$ for all $T_j \in \mathcal{T}_h$. If we sum this estimate over all elements, we are led to

$$\widetilde{\mu}_H = \|\varrho^{1/2}(1 - \Pi_h)\phi_{h/2}\|_{L^2(\Gamma)} \le \|\varrho^{1/2}(1 - \mathbb{G}_h)\phi_{h/2}\|_{L^2(\Gamma)} = \mu_H$$

which concludes the proof. □

***Remark* 5.** Theorem 3.2 states equivalence of all introduced error estimators — namely, η_H, $\widetilde{\eta}_H$, μ_H, and $\widetilde{\mu}_H$ — in case of either $d = 2$ or isotropic mesh-refinement in case of $d = 3$. However, the numerical experiments below indicate that the critical estimate $\widetilde{\eta}_H \lesssim \widetilde{\mu}_H$ does even hold for anisotropic mesh-refinement and $d = 3$. We stress that Theorem 3.4 is stronger than Theorem 3.2 in the sense that Equation (3.7) implies (3.5). □

***Remark* 6.** Note that the L^2-projection Π_h onto $\mathcal{P}^0(\mathcal{T}_h)$ for $\mathcal{T}_h = \{T_1, \dots, T_N\}$ reads

$$(\Pi_h v)|_T = \frac{1}{|T|} \int_T v\, ds \quad \text{for all } v \in L^2(\Gamma) \text{ and } T \in \mathcal{T}_h, \tag{3.8}$$

where $|T|$ denotes the surface measure of $T \in \mathcal{T}_h$. Thus, $\widetilde{\mu}_H$ can be computed in real linear complexity $\mathcal{O}(N)$ with $N = \#\mathcal{T}_h$ the number of elements of $\mathcal{T}_h$. Note that the new estimators only affect step (ii) of Algorithm 3.3: We now compute the Galerkin solution $\phi_{h/2}^{(\ell)} \in \mathcal{P}^0(\mathcal{T}_{h/2}^{(\ell)})$ and then define $\phi_h^{(\ell)} := \Pi_h^{(\ell)} \phi_{h/2}^{(\ell)}$, where $\Pi_h^{(\ell)}$ denotes the L^2-projection onto $\mathcal{P}^0(\mathcal{T}_h^{(\ell)})$. □

4. Hypersingular Integral Equation

In this section we use the same ideas as for Symm's integral equation to develop a localized h-$h/2$-error estimator for the hypersingular integral equation as well. With Ω, Γ, and $G(\cdot)$ as in the introductory section, the hypersingular integral equation reads

$$Wu = f \quad \text{on } \Gamma \tag{4.1}$$

with the hypersingular integral operator

$$Wu(x) = -\frac{\partial}{\partial n_x}\int_\Gamma u(y)\frac{\partial}{\partial n_y}G(x-y)\,ds_y \quad \text{for } x \in \Gamma. \tag{4.2}$$

Here n_x and n_y denote the outer unit normal vectors at x and y, respectively. The corresponding energy space $\mathcal{H}^{1/2}(\Gamma)$ reads, for $\alpha = 1/2$,

$$\mathcal{H}^\alpha(\Gamma) = \begin{cases} H^\alpha_0(\Gamma) = \{v \in H^\alpha(\Gamma) \,:\, \int_\Gamma v\,ds = 0\} & \text{for } \Gamma = \partial\Omega, \\ \widetilde{H}^\alpha(\Gamma) = \{v \in H^\alpha(\Gamma) \,:\, v|_{\partial\Gamma} = 0\} & \text{for } \Gamma \subsetneqq \partial\Omega, \end{cases} \tag{4.3}$$

where $\alpha \in [0,1]$. With $\mathcal{H}^{-1/2}(\Gamma) = (\mathcal{H}^{1/2}(\Gamma))^*$, the hypersingular integral operator, $W : \mathcal{H}^{1/2}(\Gamma) \to \mathcal{H}^{-1/2}(\Gamma)$ is an elliptic isomorphism and thus provides an equivalent scalar product

$$\langle\!\langle u\,, v\rangle\!\rangle = \langle Wu\,, v\rangle \quad \text{for } u, v \in \mathcal{H}^{1/2}(\Gamma) \tag{4.4}$$

with induced energy norm $|||\cdot||| \sim \|\cdot\|_{H^{1/2}(\Gamma)}$ on $\mathcal{H}^{1/2}(\Gamma)$.

Let $\mathcal{T}_h$ be a regular triangulation of Γ and define

$$\mathcal{S}^1_0(\mathcal{T}_h) := \begin{cases} \{v_h \in \mathcal{S}^1(\mathcal{T}_h) \,:\, \int_\Gamma v_h\,ds = 0\} & \text{for } \Gamma = \partial\Omega, \\ \{v_h \in \mathcal{S}^1(\mathcal{T}_h) \,:\, v_h|_{\partial\Gamma} = 0\} & \text{for } \Gamma \subsetneqq \partial\Omega, \end{cases} \tag{4.5}$$

where $\mathcal{S}^1(\mathcal{T}_h) := \mathcal{P}^1(\mathcal{T}_h) \cap C(\Gamma)$ consists of all $\mathcal{T}_h$-piecewise affine and globally continuous splines. Then, $\mathcal{S}^1_0(\mathcal{T}_h)$ is a subspace of $\mathcal{H}^1(\Gamma)$ and hence of $\mathcal{H}^{1/2}(\Gamma)$.

Given $f \in \mathcal{H}^{-1/2}(\Gamma)$, let $u \in \mathcal{H}^{1/2}(\Gamma)$ denote the exact solution of (4.1) and $u_h \in \mathcal{S}^1_0(\mathcal{T}_h)$ (resp. $u_{h/2}$) be the Galerkin solution of (4.1), i.e.

$$\langle\!\langle u_h\,, v_h\rangle\!\rangle = \langle f\,, v_h\rangle \quad \text{for all } v_h \in \mathcal{S}^1_0(\mathcal{T}_h). \tag{4.6}$$

According to Proposition 1.1, the h-$h/2$-error estimator

$$\eta_H = |||u_h - u_{h/2}||| \tag{4.7}$$

is efficient with constant $C_{\rm eff} = 1$. Moreover, under the saturation assumption

$$|||u - u_{h/2}||| \le q\,|||u - u_h|||, \tag{A}$$

for some $q \in (0,1)$, we obtain reliability with constant $C_{\rm rel} = 1/\sqrt{1-q^2}$.

Lemma 4.1 below provides a localization of the $\mathcal{H}^{1/2}$-norm for H^1-conforming discrete functions. This localization is given in terms of a mesh-size weighted H^1-seminorm, where $\nabla(\cdot)$ denotes the surface gradient. For $d = 2$, $\nabla(\cdot)$ coincides with the arc-length derivative $(\cdot)' := d/ds$.

The inverse estimate (4.12) is proven in [CP3, FFP]. For the approximation estimate (4.13), let $\mathcal{A}_h$ be a Clément-type approximation operator, i.e. an operator defined on $H^1(\Gamma)$ which satisfies the following three properties (4.8)–(4.10) with constants $C_6, C_7 > 0$ that do not depend on $v \in H^1(\Gamma)$: First, H^1-stability

$$\|\nabla(v - \mathcal{A}_h v)\|_{L^2(\Gamma)} \le C_6\,\|\nabla v\|_{L^2(\Gamma)}. \tag{4.8}$$

Second, a first-order approximation property with respect to the L^2-norm

$$\|v - \mathcal{A}_h v\|_{L^2(\Gamma)} \le C_7\,\|h\nabla v\|_{L^2(\Gamma)}. \tag{4.9}$$

Finally, we assume that $\mathcal{A}_h$ maps into the right discrete space, namely

$$\mathcal{A}_h v \in \mathcal{S}^1_0(\mathcal{T}_h). \tag{4.10}$$

In case of $\Gamma \subsetneq \partial\Omega$ this is usually satisfied by definition of $\mathcal{A}_h$. In case of $\Gamma = \partial\Omega$, one simply modifies $\mathcal{A}_h$ by subtracting the integral mean, which does not change (4.8)–(4.9), c.f. [FFP]. Under the latter assumptions (4.8)–(4.10), one can employ interpolation techniques to derive the approximation estimate (4.13).

We stress the Scott-Zhang projection operator as one prominent example for a Clément-type operator. The Scott-Zhang operator additionally satisfies the projection property

$$\mathcal{A}_h^2 = \mathcal{A}_h. \tag{4.11}$$

As above, the improved estimates (4.14)–(4.15) are immediate consequences of (4.13) and the projection property.

Lemma 4.1. (i) *For any discrete function $v_h \in \mathcal{S}^1_0(\mathcal{T}_h)$ holds the inverse estimate*

$$\|\varrho^{1/2}\nabla v_h\|_{L^2(\Gamma)} \le C_8 |\!|\!| v_h |\!|\!|, \tag{4.12}$$

where the constant $C_8 > 0$ depends only on Γ and $\kappa(\mathcal{T}_h)$.
(ii) *For any Clément-type approximation operator $\mathcal{A}_h$ onto $\mathcal{S}^1_0(\mathcal{T}_h)$ and any $v \in \mathcal{H}^1(\Gamma)$ holds*

$$|\!|\!| v - \mathcal{A}_h v |\!|\!| \le C_9 \, \|h^{1/2}\nabla v\|_{L^2(\Gamma)}, \tag{4.13}$$

where the constant $C_9 > 0$ depends only on Γ and the constants $C_6, C_7 > 0$.
(ii) *In particular, the Scott-Zhang projection $\mathcal{A}_h$ onto $\mathcal{S}^1_0(\mathcal{T}_h)$ satisfies, for $v \in \mathcal{H}^1(\Gamma)$,*

$$|\!|\!| v - \mathcal{A}_h v |\!|\!| \le C_9 \min\big\{\|h^{1/2}\nabla(v - \mathcal{A}_h v)\|_{L^2(\Gamma)}, \|h^{1/2}\nabla v\|_{L^2(\Gamma)}\big\}. \tag{4.14}$$

(iii) *For $\mathbb{G}_h$ the Galerkin projection onto $\mathcal{S}^1_0(\mathcal{T}_h)$ and any $v \in L^2(\Gamma)$ holds*

$$|\!|\!| v - \mathbb{G}_h v |\!|\!| \le C_9 \min\big\{\|h^{1/2}\nabla(v - \Pi_h v)\|_{L^2(\Gamma)}, \|h^{1/2}\nabla v\|_{L^2(\Gamma)}\big\}. \tag{4.15}$$

□

***Remark* 7.** We remark that, by theory, the constants C_6 and C_7 — and consequently also C_9 — usually depend on the shape-regularity constant $\sigma(\mathcal{T}_h)$, which contradicts an anisotropic mesh-refinement. □

The following theorem now provides a localized version μ_H of η_H.

Theorem 4.2. *The a posteriori error estimator*

$$\mu_H = \|\varrho^{1/2}\nabla(u_h - u_{h/2})\|_{L^2(\Gamma)} \tag{4.16}$$

satisfies

$$(\sqrt{2}\, C_8)^{-1}\mu_H \le \eta_H \le C_9 \, \sigma(\mathcal{T}_h)^{1/2} \, \mu_H \tag{4.17}$$

with the constants C_8, C_9 from Lemma 4.1. In particular μ_H is always efficient.

Proof. Note that $\mathcal{S}^1_0(\mathcal{T}_h) \subset \mathcal{S}^1_0(\mathcal{T}_{h/2})$ implies $\mathbb{G}_h u_{h/2} = u_h$, which leads to

$$u_h - u_{h/2} = (1 - \mathbb{G}_h)(u_h - u_{h/2}).$$

Therefore, the approximation property (4.15) yields $\eta_H \le C_9 \mu_H$. For the converse estimate $\mu_H \le \sqrt{2}\, C_8 \, \eta_H$, we apply the local inverse estimate (4.12), which concludes the proof. □

As for Symm's integral, the following theorems aim to avoid the computation of u_h and replace u_h by some cheap approximation $\mathcal{A}_h u_{h/2}$ of $u_{h/2}$, where we use the Scott-Zhang projection which can be computed in linear complexity.

Theorem 4.3. *With $\mathcal{A}_h : \mathcal{H}^1(\Gamma) \to \mathcal{S}^1_0(\mathcal{T}_h)$ the Scott-Zhang projection, we define the error estimators*

$$\widetilde{\eta}_H := |||u_{h/2} - \mathcal{A}_h u_{h/2}||| \quad \text{and} \quad \widetilde{\mu}_H := \|h^{1/2}\nabla(u_{h/2} - \mathcal{A}_h u_{h/2})\|_{L^2(\Gamma)}. \tag{4.18}$$

Then, there holds

$$\widetilde{\mu}_H \le \sqrt{2}\, C_8\, \widetilde{\eta}_H \quad \text{and} \quad \eta_H \le \widetilde{\eta}_H \le C_9\, \sigma(\mathcal{T}_h)^{1/2}\, \widetilde{\mu}_H \tag{4.19}$$

with the constants $C_8, C_9 > 0$ from Lemma 4.1.

Proof. The estimate $\eta_H \le \widetilde{\eta}_H$ follows from the bestapproximation property of $\mathbb{G}_h$, namely $|||(1-\mathbb{G}_h)v||| \le |||(1-\mathcal{A}_h)v|||$ for all $v \in \mathcal{H}^{1/2}(\Gamma)$. The estimate $\widetilde{\eta}_H \le C_9\, \widetilde{\mu}_H$ follows from (4.13), the estimate $\widetilde{\mu}_H \le \sqrt{2}\, C_8 \widetilde{\eta}_H$ follows from (4.12). □

***Remark* 8.** We stress that Theorem 4.3 is suboptimal in the sense that we did not succeed to prove the estimate $\widetilde{\mu}_H \lesssim \mu_H$, which would have implied efficiency of $\widetilde{\mu}_H$. Equivalency of $\widetilde{\eta}_H$ and $\widetilde{\mu}_H$ hold at least for $d = 2$ and isotropic mesh-refinement for $d = 3$. □

For two dimensions, we can provide the following improved result, which corresponds to Theorem 3.4 for Symm's integral equation.

Theorem 4.4. *Provided $\Omega \subset \mathbb{R}^2$, let $\widehat{I}_h v := \sum_{z\in\mathcal{N}} v(z)\phi_z$ denote the nodal interpolation operator $\widehat{I}_h : \mathcal{C}(\Gamma) \to \mathcal{S}^1(\mathcal{T})$ and define*

$$I_h : \mathcal{H}^1(\Gamma) \to \mathcal{S}^1_0(\mathcal{T}), \quad I_h v := \begin{cases} \widehat{I}_h v & \text{for } \Gamma \subsetneqq \partial\Omega, \\ \widehat{I}_h v - |\Gamma|^{-1} \int_\Gamma \widehat{I}_h v\, ds & \text{for } \Gamma = \partial\Omega. \end{cases} \tag{4.20}$$

We consider the error estimators

$$\widehat{\eta}_H := |||u_{h/2} - I_h u_{h/2}||| \quad \text{and} \quad \widehat{\mu}_H := |||h^{1/2}(u_{h/2} - I_h u_{h/2})'|||. \tag{4.21}$$

Then, there holds equivalence of $\widehat{\eta}_H$ and $\widehat{\mu}_H$ with η_H and μ_H, namely

$$\widehat{\mu}_H \le \mu_H \le C_8 \eta_H. \quad \text{and} \quad \eta_H \le \widehat{\eta}_H \le C_{10}\widehat{\mu}_H \tag{4.22}$$

Here, C_8 denotes the constant from Lemma 4.1. The constant $C_{10} > 0$ only depends on Γ and $\kappa(\mathcal{T}_h)$, but neither on h nor on the number $\#\mathcal{T}_h$ of elements. In particular, $\widehat{\eta}_H$ and $\widehat{\mu}_H$ are always efficient.

Proof. The estimate $\eta_H \le \widehat{\eta}_H$ follows from the bestapproximation property of the Galerkin projection. For the verification of $\widehat{\eta}_H \le C_{10}\widehat{\mu}_H$, the reader is referred to [CP3, Corollary 3.5]. It thus only remains to prove $\widehat{\mu}_H \le \mu_H$: For $v \in \mathcal{H}^1(\Gamma)$ and $w := v - I_h v$, there holds

$$\int_{T_j} v' - (I_h v)'\, ds = \int_{T_j} w'\, ds = 0,$$

since $w(z) = w(\zeta)$ for all nodes $z, \zeta \in \mathcal{N}$. Together with $(I_h v)' \in \mathcal{P}^0(T_j)$, this implies the identity $(I_h v)' = \Pi_h v'$, where $\Pi_h : L^2(T_j) \to \mathcal{P}^0(T_j)$ is the (elementwise) L^2-orthogonal projection onto piecewise constant functions. Said differently, we have

$$\|v' - (I_h v)'\|_{L^2(T_j)} = \min_{\lambda\in\mathbb{R}} \|v' - \lambda\|_{L^2(T_j)} \quad \text{for all } T_j \in \mathcal{T}_h.$$

A summation of these estimates over all elements $T_j \in \mathcal{T}_h$ yields

$$\|h^{1/2}(v - I_h v)'\|_{L^2(\Gamma)} = \min_{p_h \in \mathcal{P}^0(\mathcal{T}_h)} \|h^{1/2}(v' - p)\|_{L^2(\Gamma)} \le \|h^{1/2}(v - \mathbb{G}_h v)'\|_{L^2(\Gamma)}.$$

Plugging-in $v = u_{h/2}$, we conclude the proof. □

We stress some observations from the proof of the last theorem and the extension of the result to 3D.

***Remark* 9.** The H^1-seminorm $|v|_{H^1(\Gamma)} = \|\nabla v\|_{L^2(\Gamma)}$ is an equivalent norm on $\mathcal{H}^1(\Gamma)$. Let $\mathbb{P}_h : \mathcal{H}^1(\Gamma) \to \mathcal{S}^1_0(\Gamma)$ denote the orthogonal projection with respect to $|\cdot|_{H^1(\Gamma)}$. In the latter proof we have seen that, for $d = 2$, there holds $\mathbb{P}_h = I_h$ as well as $(\mathbb{P}_h v)' = \Pi_h v'$, where Π_h denotes the L^2-projection onto $\mathcal{P}^0(\mathcal{T}_h)$. Therefore, the error estimators

$$\widehat{\mu}_H^{(1)} = \|\varrho^{1/2}(\nabla u_{h/2} - \nabla \mathbb{P}_h u_{h/2})\|_{L^2(\Gamma)} \quad \text{resp.} \quad \widehat{\mu}_H^{(2)} = \|\varrho^{1/2}(\nabla u_{h/2} - \Pi_h \nabla u_{h/2})\|_{L^2(\Gamma)}$$

coincide with $\widehat{\mu}_H$ for 2D. For 3D, neither of the two representations of $\mathbb{P}_h$ (resp. I_h) hold. However, one may nevertheless consider the error estimators $\mu_H^{(j)}$:
(a) From $\nabla \mathbb{G}_h u_{h/2} \in \mathcal{P}^0(\mathcal{T}_h)$, we derive the general efficiency estimate $\widehat{\mu}_H^{(2)} \le \mu_H$.
(b) The estimate $|u_{h/2} - \mathbb{P}_h u_{h/2}|_{H^1(\Gamma)} \le |u_{h/2} - \mathbb{G}_h u_{h/2}|_{H^1(\Gamma)}$ yields equivalency of estimators $\widehat{\mu}_H^{(1)} \le \mu_H \lesssim \eta_H \le |\!|\!| u_{h/2} - \mathbb{P}_h u_{h/2} |\!|\!| \lesssim \widehat{\mu}_H^{(1)}$ at least for uniform mesh-refinement.
(c) Finally, the authors did not succeed to verify any improved estimates for 3D. □

5. Integral Equation for a Transmission Problem

This section is devoted to a transmission problem which involves the integral operators of Section 3 and 4. Given $(f, g) \in H^{1/2}(\Gamma) \times H^{-1/2}(\Gamma)$ along the boundary $\Gamma = \partial\Omega$ of a bounded Lipschitz domain $\Omega \subset \mathbb{R}^d$, the strong form of the transmission problem reads: Find $u^- \in H^1(\Omega)$ and $u^+ \in H^1_{\ell oc}(\mathbb{R}^d \backslash \overline{\Omega})$ with

$$\Delta u^- = 0 \text{ in } \Omega \quad \text{as well as} \quad \Delta u^+ = 0 \text{ in } \mathbb{R}^d \backslash \overline{\Omega} \tag{5.1}$$

with some radiation condition on u^+ at infinity and jump conditions

$$u^- = u^+ + f \quad \text{and} \quad \frac{\partial u^-}{\partial n} = \frac{\partial u^+}{\partial n} + g \quad \text{on } \Gamma. \tag{5.2}$$

This is equivalently formulated by the boundary integral equation [CS]

$$A \begin{pmatrix} u \\ \phi \end{pmatrix} = \left(\frac{1}{2} + A \right) \begin{pmatrix} f \\ g \end{pmatrix} \quad \text{in } \mathcal{H} \subset H^{1/2}(\Gamma) \times H^{-1/2}(\Gamma) \tag{5.3}$$

with the Calderón projector

$$A = \begin{pmatrix} -K & V \\ W & K' \end{pmatrix}. \tag{5.4}$$

The simple-layer potential operator V is defined in (1.1), and the hypersingular integral operator W is defined in (4.2). Moreover, K denotes the double-layer potential operator and

K' its adjoint defined by

$$K : H^{1/2}(\Gamma) \to H^{1/2}(\Gamma), \qquad Kv(x) = \int\!\!\!\!\!\!-_\Gamma v(y) \frac{\partial}{\partial n_y} G(x-y)\, ds_y, \tag{5.5}$$

$$K' : H^{-1/2}(\Gamma) \to H^{-1/2}(\Gamma), \qquad K'\phi(x) = \int\!\!\!\!\!\!-_\Gamma \phi(y) \frac{\partial}{\partial n_x} G(x-y)\, ds_y, \tag{5.6}$$

with kernel $G(\cdot)$ from (1.3). Here, $\int\!\!\!\!\!\!-_\Gamma ds$ denotes the Cauchy principal value and $\partial/\partial n_z$ denotes the normal derivative with respect to the z-variable. As above, duality is understood with respect to the extended L^2 scalar product,

$$\langle \begin{pmatrix} u \\ \phi \end{pmatrix}, \begin{pmatrix} v \\ \psi \end{pmatrix} \rangle_{\mathcal{H}} = \langle u, \psi \rangle + \langle v, \phi \rangle \quad \text{for } (u,\phi),(v,\psi) \in \mathcal{H} := H^{1/2}_0(\Gamma) \times H^{-1/2}_0(\Gamma), \tag{5.7}$$

where $H^{1/2}_0(\Gamma)$ is defined in (4.3) and $H^{-1/2}_0(\Gamma) := H^{1/2}_0(\Gamma)^* = \{\psi \in H^{-1/2}(\Gamma) : \langle \psi, 1\rangle = 0\}$.

The mapping properties of the involved boundary operators [McL] show that $A : \mathcal{H} \to \mathcal{H}$ is continuous and $\mathcal{H}$-elliptic with respect to the canonical norm $\|(v,\psi)\|^2_{\mathcal{H}} := \|v\|^2_{H^{1/2}(\Gamma)} + \|\psi\|^2_{H^{-1/2}(\Gamma)}$. In fact, elementary calculations show that the (non-symmetric) bilinear form

$$\langle\!\langle (u,\phi), (v,\psi) \rangle\!\rangle = \langle A \begin{pmatrix} u \\ \phi \end{pmatrix}, \begin{pmatrix} v \\ \psi \end{pmatrix} \rangle_{\mathcal{H}}, \tag{5.8}$$

induces an equivalent energy norm $|||\cdot|||$ which satisfies

$$|||(u,\phi)|||^2 = \langle\!\langle (u,\phi), (u,\phi) \rangle\!\rangle = \|\phi\|^2_V + \|u\|^2_W \quad \text{for all } (u,\phi) \in \mathcal{H} \tag{5.9}$$

with the energy norms $\|\cdot\|_V$ and $\|\cdot\|_W$ from Section 3 and 4, respectively. Note that $|||\cdot|||$ is indeed a Hilbert norm, but $\langle\!\langle \cdot, \cdot \rangle\!\rangle$ is *not* the corresponding scalar product!

For a regular triangulation $\mathcal{T}_h$ of Γ, we consider the discrete space

$$\mathcal{S}^1_0(\mathcal{T}_h) \times \mathcal{P}^0_0(\mathcal{T}_h),$$

where $\mathcal{P}^p_0(\mathcal{T}_h) := \{\psi_h \in \mathcal{P}^p(\mathcal{T}_h) : \int_\Gamma \psi_h\, ds = 0\}$. Let $(u_h, \phi_h) \in \mathcal{S}^1_0(\mathcal{T}_h) \times \mathcal{P}^0_0(\mathcal{T}_h)$ and $(u_{h/2}, \phi_{h/2}) \in \mathcal{S}^1_0(\mathcal{T}_{h/2}) \times \mathcal{P}^0_0(\mathcal{T}_{h/2})$ be two Galerkin solutions, where $\mathcal{T}_{h/2}$ is obtained from a uniform refinement of $\mathcal{T}_h$. We define the canonical error estimators

$$\begin{aligned} \eta_H &:= |||(u_{h/2}, \phi_{h/2}) - (u_h, \phi_h)|||, \\ \mu_H &:= \big(\|\varrho^{1/2} \nabla (u_{h/2} - u_h)\|^2_{L^2(\Gamma)} + \|\varrho^{1/2}(\phi_{h/2} - \phi_h)\|^2_{L^2(\Gamma)} \big)^{1/2}, \end{aligned} \tag{5.10}$$

as well as

$$\begin{aligned} \widetilde{\eta}_H &:= |||(u_{h/2}, \phi_{h/2}) - (\mathcal{A}_h u_{h/2}, \Pi_h \phi_{h/2})|||, \\ \widetilde{\mu}_H &:= \big(\|\varrho^{1/2} \nabla (u_{h/2} - \mathcal{A}_h u_{h/2})\|^2_{L^2(\Gamma)} + \|\varrho^{1/2}(\phi_{h/2} - \Pi_h \phi_{h/2})\|^2_{L^2(\Gamma)} \big)^{1/2}, \end{aligned} \tag{5.11}$$

where Π_h is the L^2-projection onto $\mathcal{P}^0_0(\mathcal{T}_h)$ and where $\mathcal{A}_h$ denotes either the Scott-Zhang projection onto $\mathcal{S}^1_0(\mathcal{T}_h)$ for $d = 3$ or the nodal interpolation operator for $d = 2$. We stress that η_H is always efficient, whereas reliability holds under the saturation assumption.

Theorem 5.1. *We have the following relations between the four error estimators, where the involved constants read* $C_{11} := \max\{C_3, C_8\}$ *and* $C_{12} := \max\{C_4, C_9\}$*:*
(i) $C_{11}^{-1}\, \mu_H \le \eta_H \le C_{12}\, \sigma(\mathcal{T}_h)^{1/2}\, \mu_H$.
(ii) $C_{11}^{-1}\, \widetilde{\mu}_H \le \widetilde{\eta}_H \le C_{12}\, \sigma(\mathcal{T}_h)^{1/2}\, \widetilde{\mu}_H$ *as well as* $\eta_H \le \widetilde{\eta}_H$.
(iii) *For* $d = 2$, *holds* $\widetilde{\mu}_H \le \mu_H \le C_{11} \eta_H$ *and* $\eta_H \le \widetilde{\eta}_H \le C_{12}\, \widetilde{\mu}_H$.

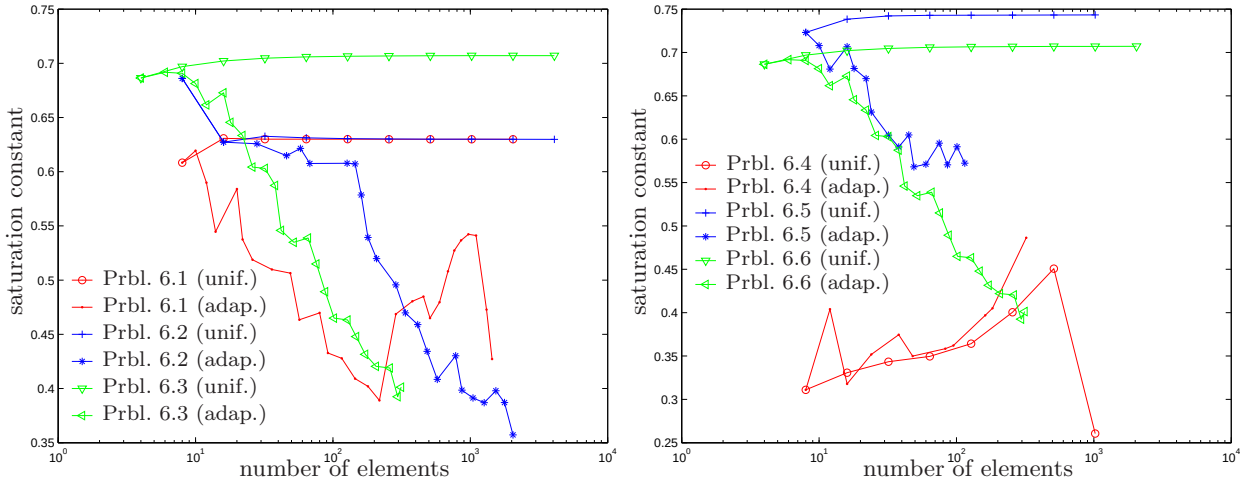

FIGURE 1. Experimental saturation constant $q = |||\phi - \phi_{h/2}|||/|||\phi - \phi_h|||$ for Symm's integral equation of Dirichlet Problem 6.1, Capacity Problem 6.2, and Slit Problem 6.3 for uniform and $\widetilde{\mu}_H$-adaptive mesh-refinement (left). Experimental saturation constant $q = |||u - u_{h/2}|||/|||u - u_h|||$ for hypersingular integral equation of Neumann Problem 6.4 and 6.5 and Slit Problem 6.6 for uniform and $\widetilde{\mu}_H$-adaptive mesh-refinement (right). In any case holds $q < 1$, which yields reliability of η_H.

Proof. For the L^2-projection $\widehat{\Pi}_h$ onto $\mathcal{P}^0(\mathcal{T}_h)$ holds

$$0 = \langle \psi - \widehat{\Pi}_h \psi \,, 1\rangle = -\langle \widehat{\Pi}_h \psi \,, 1\rangle \quad \text{for all } \psi \in L^2(\Gamma) \text{ with } \langle \psi \,, 1\rangle = 0.$$

In particular, this proves $\widehat{\Pi}_h \phi_{h/2} = \Pi_h \phi_{h/2}$. Therefore, we may simply apply Theorem 3.4, and Theorem 4.2–4.4 to conclude the proof. □

6. Numerical Experiments in 2D

This section reports on some numerical experiments in 2D to study the accuracy of the introduced error estimators and the performance of the proposed adaptive strategy.

Examples 6.1–6.3 consider Symm's integral equation from Section 3. They have been realized and studied in [CP1] for adaptive mesh-refinement with respect to the residual-based error estimator introduced by Faermann [F1]. Example 6.1 considers Symm's integral equation corresponding to a Dirichlet problem on the L-shaped domain with reentrant corner at the origin. The exact solution of the PDE is given in polar coordinates by $U(r, \varphi) = r^\alpha \cos(\alpha\varphi)$ and has a generic singularity with $\alpha = 2/3$ at the reentrant corner $(0, 0)$, where the interior angle is $3\pi/2$. Example 6.2 deals with Symm's integral equation with a constant right-hand side to exclude positive and negative effects due to quadrature errors. The exact solution is unknown. The sequence of discrete solutions shows singularities at the five convex corners of the L-shape. Example 6.3, taken from [ChS], considers a slit problem, where the known exact solution only belongs to $H^{-\varepsilon}(\Gamma)\backslash L^2(\Gamma)$ for all $\varepsilon > 0$.

Examples 6.4–6.6 from [CP3] consider the hypersingular integral equation from Section 4. Example 6.4 treats the Neumann problem on the L-shaped domain with the same exact solution of the corresponding PDE as for Example 6.1. Whereas the exact solution of Symm's

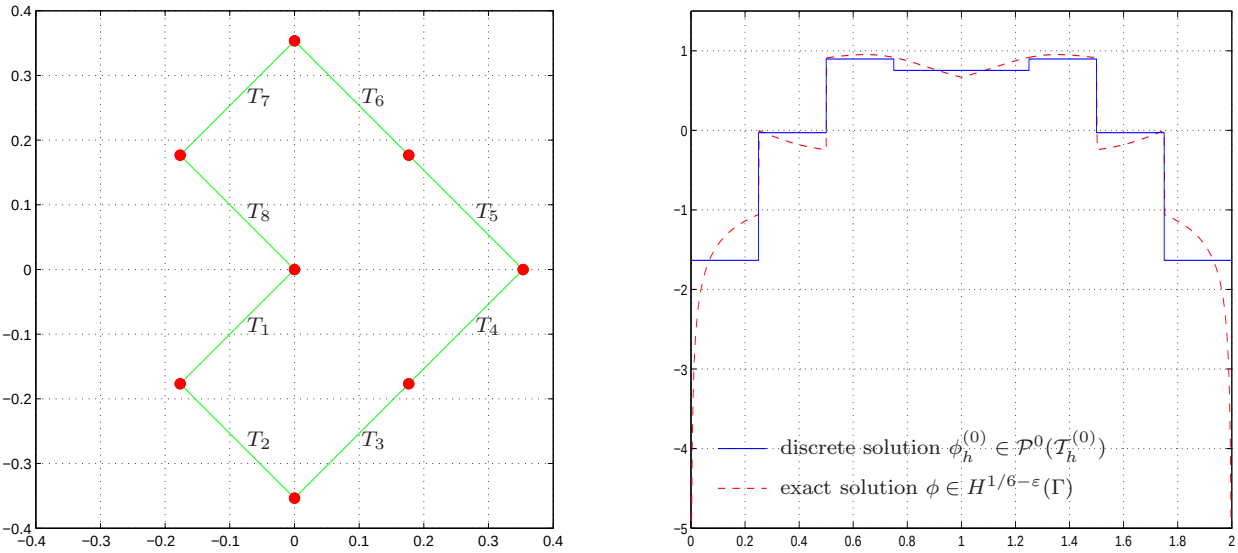

FIGURE 2. Initial mesh $\mathcal{T}_h^{(0)}$ with $N = 8$ elements (left) in Example 6.1 and 6.2 and corresponding discrete solution $\phi_h^{(0)} \in \mathcal{P}^0(\mathcal{T}_h^{(0)})$ in Dirichlet Problem 6.1 (right) plotted over the arc-length s, where $s(0) = s(2)$ corresponds to the reentrant corner $(0,0) \in \Gamma$. For comparison, the right figure even shows the exact solution $\phi \in H^{1/6-\varepsilon}(\Gamma)$.

integral equation is singular, the solution of the hypersingular equation appears to be piecewise smooth in this case. We observe that uniform mesh-refinement leads to the optimal order of convergence. In Example 6.5, we therefore consider the same example with stronger singularity due to the choice $\alpha = 3/7$. Then, the Dirichlet data are singular at the reentrant corner, and uniform mesh-refinement shows a suboptimal convergence rate for the numerical solution of the hypersingular integral equation. Finally, Example 6.6 considers a slit problem. The exact solution has limited smoothness and belongs to $\widetilde{H}^{1-\varepsilon}(\Gamma)\backslash H^1(\Gamma)$ for any $\varepsilon > 0$.

Remarks on the implementation of Symm's integral equation are found in the statement of Example 6.1, whereas details on the implementation of the hypersingular integral equation are part of the statement of Example 6.4.

Figure 1 shows the experimental saturation constant $q = |||\phi - \phi_{h/2}|||/|||\phi - \phi_h|||$ for Examples 6.1–6.1 as well as $q = |||u - u_{h/2}|||/|||u - u_h|||$ for Examples 6.4–6.6 for both, uniform and adaptive mesh-refinement. We stress that in any case, $q < 0.75$ is uniformly bounded from 1, which empirically proves reliability of the h-$h/2$-error estimator η_H.

6.1. Symm's Integral Equation for Dirichlet Problem on L-Shaped Domain. We consider the Dirichlet problem

$$-\Delta U = 0 \quad \text{in } \Omega \quad \text{with boundary conditions} \quad U = g \quad \text{on } \Gamma := \partial\Omega \tag{6.1}$$

on the L-shaped domain $\Omega \subset \mathbb{R}^2$ shown in Figure 2 with known exact solution

$$U(x) = r^\alpha \cos(\alpha\varphi) \quad \text{in polar coordinates} \quad x = r\,(\cos\varphi, \sin\varphi) \tag{6.2}$$

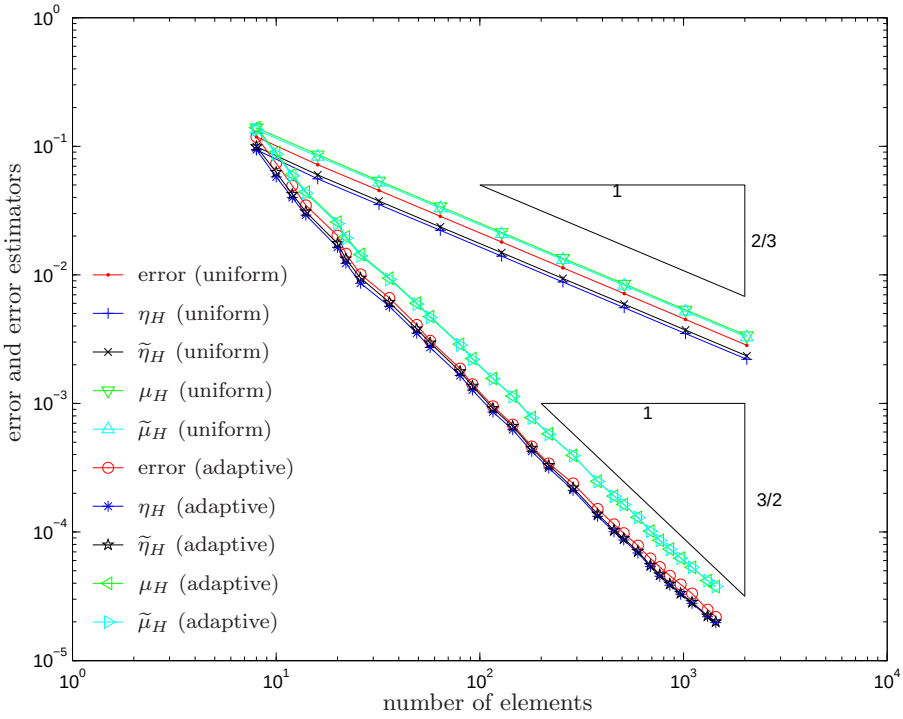

FIGURE 3. Error $|||\phi - \phi_h|||$ and error estimators η_H, $\widetilde{\eta}_H$, μ_H, $\widetilde{\mu}_H$ in Dirichlet Problem 6.1 on L-shaped domain for uniform and $\widetilde{\mu}_H$-adaptive mesh-refinement.

for some fixed parameter $\alpha > 0$. With V the simple-layer and K the double-layer potential of Equation (1.2) and (5.5), respectively, Symm's integral equation

$$V\phi = (1/2 + K)g \tag{6.3}$$

is an equivalent formulation of the Dirichlet problem (6.2), c.f. [McL]. The unique solution $\phi \in H^{-1/2}(\Gamma)$ of (6.3) is the normal derivative $\phi = \partial U/\partial n$, which reads in polar coordinates

$$\phi(x) = (w \cdot n(x))\, \alpha r^{\alpha-1} \quad \text{with } w := \begin{pmatrix} \cos(\varphi)\cos(\alpha\varphi) + \sin(\varphi)\sin(\alpha\varphi) \\ \sin(\varphi)\cos(\alpha\varphi) - \cos(\varphi)\sin(\alpha\varphi) \end{pmatrix} \in \mathbb{R}^2. \tag{6.4}$$

For the first numerical experiment, we choose $\alpha = 2/3$. The Dirichlet problem then leads to $U \notin H^2(\Omega)$ with a generic singularity at the reentrant corner.

The implementation of Symm's integral equation has been done as follows: For a given triangulation $\mathcal{T}_h = \{T_1, \ldots, T_N\}$ of Γ, we used the set of characteristic functions $\mathcal{B} := \{\chi_T : T \in \mathcal{T}_h\}$ as a basis of $\mathcal{P}^0(\mathcal{T}_h)$. The entries

$$\mathbf{A}_{jk} = \langle V\chi_{T_j}, \chi_{T_k} \rangle$$

of the Galerkin matrix $\mathbf{A} \in \mathbb{R}^{N\times N}_{sym}$ are computed analytically [M]. To compute the entries of the load vector $\mathbf{b} \in \mathbb{R}^n$, we use

$$\mathbf{b}_j = \langle (1/2 + K)g, \chi_{T_j} \rangle = \langle g, (1/2 + K')\chi_{T_j} \rangle = \frac{1}{2}\int_{T_j} g\, ds + \sum_{k=1}^{N} \int_{T_k} g(x) K^* \chi_{T_j}(x)\, ds_x.$$

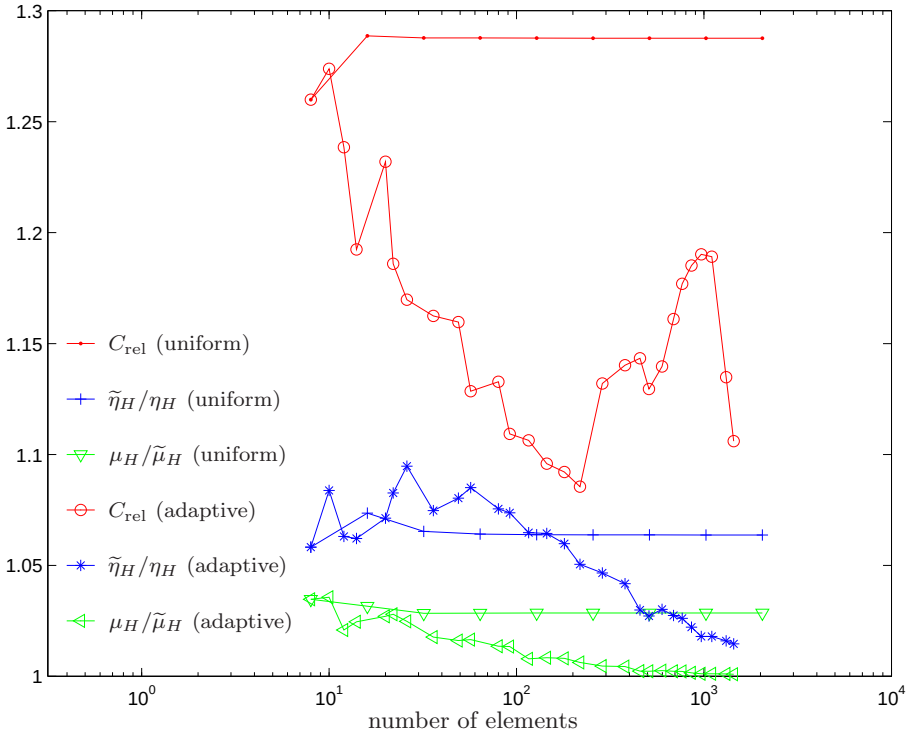

FIGURE 4. Experimental reliability constant $C_{\rm rel} = |||\phi - \phi_h|||/\eta_H$ as well as quotients $\eta_H/\widetilde{\eta}_H$ and $\widetilde{\mu}_H/\mu_H$ in Dirichlet Problem 6.1 for uniform and $\widetilde{\mu}_H$-adaptive mesh-refinement.

The first integral is computed by Gauss quadrature. Although $\texttt{adlp}(T_j;x) := (K^*\chi_{T_j})(x)$ can be computed via an analytic formula, it leads to weak singularities for x near T_j. For a neighbouring element T_k, we thus use an explicit decomposition

$$\texttt{adlp}(T_j;x) = a\,\log(|x-b|/|x-c|) + \text{smooth}(x)$$

for some parameters a, b, and c to obtain

$$\int_{T_k} g(x)\,\texttt{adlp}(T_j;x)\,ds_x = \int_0^1 g(\gamma(s))\,\log s\,ds + \int_{T_k} g(x)\,\text{smooth}(x)\,ds_x.$$

The first integral is computed with a weighted Gauss quadrature rule, whereas the other integral involves a smooth integrand and is hence approximated by simple Gauss quadrature. Throughout, we found that the use of quadrature rules of order 7 was sufficient. The discrete solution $\phi_h \in \mathcal{P}^0(\mathcal{T}_h)$ then reads $\phi_h = \sum_{j=1}^N \mathbf{x}_j\chi_{T_j}$, where $\mathbf{x} \in \mathbb{R}^N$ is the solution of the linear system $\mathbf{A}\mathbf{x} = \mathbf{b}$.

All experiments are performed by use of Algorithm 3.3, where we choose either $\theta = 0$ for uniform or $\theta = 0.5$ for adaptive mesh-refinement. For the marking step (v) in Algorithm 3.3, we use the local contributions

$$\widetilde{\mu}_{H,j} = h_j^{1/2}\|\phi_{h/2} - \Pi_h\phi_{h/2}\|_{L^2(T_j)}$$

of $\widetilde{\mu}_H$ in case of adaptive mesh-refinement. Here Π_h denotes the L^2-projection onto $\mathcal{P}^0(\mathcal{T}_h)$. To control the K-mesh property of the adaptively generated meshes $\mathcal{T}_h^{(\ell)}$, we further mark

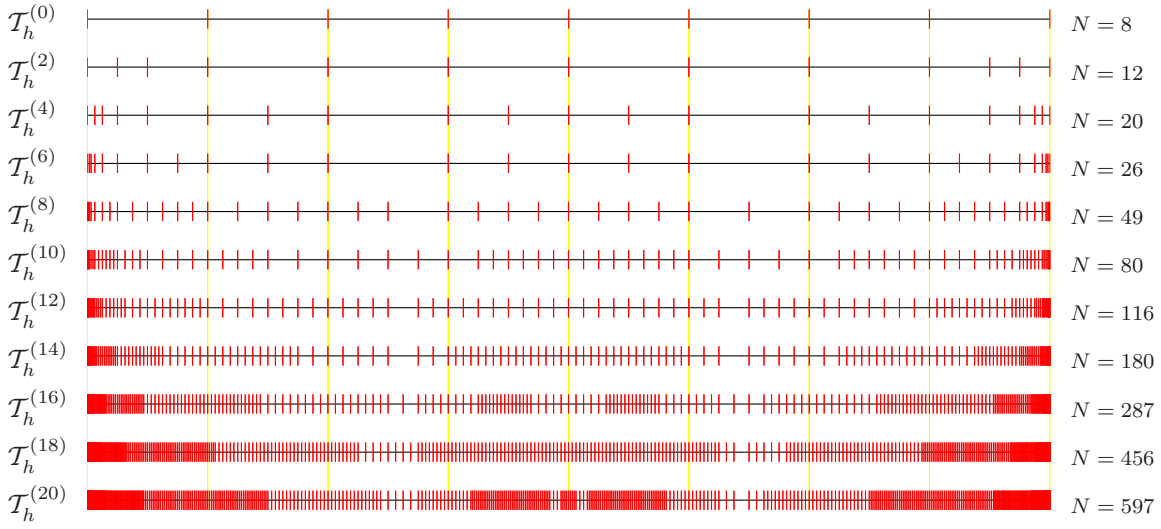

FIGURE 5. $\widetilde{\mu}_H$-adaptively generated meshes in Dirichlet Problem 6.1 plotted over the arclength $s = 0, \dots, 2$. The mesh-size of the uniform initial mesh $\mathcal{T}_h^{(0)}$ is $h = 1/4$. For the finest mesh $\mathcal{T}_h^{(20)}$ shown, the local mesh-size varies between $h_{\max} = 2^{-5}$ and $h_{\min} = 2^{-22}$. The singularity of ϕ at the reentrant corner is reflected by a strong refinement at arclength $s = 0$ and $s = 2$ by periodicity.

the neighbours $T_k \in \mathcal{T}_h^{(\ell-1)}$ of an already marked element $T_j \in \mathcal{T}_h^{(\ell-1)}$ provided that $h_k > h_j$. This ensures $\kappa(\mathcal{T}_h^{(\ell)}) \le 2\kappa(\mathcal{T}_h^{(0)})$, which is important since a blow-up of the constant $\kappa(\mathcal{T}_h^{(\ell)})$ effects the constant C_3 from the inverse estimate.

The initial coarse mesh $\mathcal{T}_h^{(0)}$ with $N = 8$ equisized elements and the corresponding discrete solution $\phi_h^{(0)} \in \mathcal{P}^0(\mathcal{T}_h^{(0)})$ as well as the exact solution are visualized in Figure 2. Here, ϕ and $\phi_h^{(0)}$ are shown as plots over the arc-length. The singularity of ϕ at $(0, 0)$ is visible at arc-length parameter $s = 0$ and $s = 2$ by periodicity.

The error in the energy norm is computed by use of the Galerkin orthogonality

$$|||\phi - \phi_h||| = \big(|||\phi|||^2 - |||\phi_h|||^2\big)^{1/2}. \tag{6.5}$$

In principle, the energy $|||\phi|||^2$ of the exact solution of (6.3) can be computed analytically. However, we obtained $|||\phi|||^2$ with the help of Aitkin's Δ^2 method, where we extrapolated the energies $|||\phi_h^{(\ell)}|||^2$ for a sequence of discrete solutions on uniform meshes $\mathcal{T}_h^{(\ell)}$ with $N = 8, 16, \dots, 2048$ elements. This gives $|||\phi|||^2 = 0.4041161973$, which is used throughout in (6.5).

Besides the error, we compute the four introduced error estimators

$$\eta_H = |||\phi_{h/2} - \phi_h|||, \qquad \mu_H = \|h^{1/2}(\phi_{h/2} - \phi_h)\|_{L^2(\Gamma)},$$
$$\widetilde{\eta}_H = |||\phi_{h/2} - \Pi_h\phi_{h/2}|||, \qquad \widetilde{\mu}_H = \|h^{1/2}(\phi_{h/2} - \Pi_h\phi_{h/2})\|_{L^2(\Gamma)}.$$

We plot the Galerkin error $|||\phi - \phi_h|||$ in the energy norm and the four error estimators against the number $N = \#\mathcal{T}_h$ of elements, where the axes are scaled logarithmically. In the double-logarithmic plot, experimental convergence of order $\mathcal{O}(N^{-\alpha})$ is visible in the slope $-\alpha$ of a straight curve. Note that, for uniform mesh-refinement, the order $\mathcal{O}(N^{-\alpha})$ with respect

to the number N of elements corresponds to the order $\mathcal{O}(h^\alpha)$ with respect to the uniform mesh-size h.

From our analysis, we know that η_H is always efficient with constant $C_{\text{eff}} = 1$. Therefore, the absolute values and hence the curve of the error estimator η_H should be below the error. For 2D, Theorem 3.4 states the equivalency of the four error estimators, namely there hold the inequalities

$$\eta_H \le \widetilde{\eta}_H \lesssim \widetilde{\mu}_H \le \mu_H \lesssim \eta_H,$$

whose implications are threefold: First, the curve corresponding to η_H should always be below the curve of $\widetilde{\eta}_H$. Second, the curve corresponding to $\widetilde{\mu}_H$ should always be below the curve of μ_H. Finally, all of the four curves of the error estimators should be parallel in a certain range.

Reliability of the error estimators holds under the saturation assumption, which then implies that the error curve should be parallel to the curves of the error estimators. In Figure 1, we thus plot the experimental saturation constant $q = |||\phi - \phi_{h/2}|||/|||\phi - \phi_h|||$ and observe that $q < 0.65$ uniformly for both mesh-refining strategies.

Figure 3 provides the curves of the error and the four error estimators for both, uniform and adaptive mesh-refinement. As can be predicted from theory, we observe a suboptimal order of convergence $|||\phi - \phi_h||| = \mathcal{O}(N^{-2/3})$ for the error for uniform mesh-refinement. Moreover, all five curves are parallel, which empirically proves reliability and efficiency of all error estimators.

The adaptive mesh-refinement leads to an improvement of the convergence behaviour, namely we observe $|||\phi-\phi_h||| = \mathcal{O}(N^{-3/2})$ which is optimal in the case of $\mathcal{T}_h$-piecewise constant ansatz functions. As for uniform mesh-refinement, we observe reliability and efficiency of all error estimators in the sense that the corresponding curves are parallel.

For both refinement strategies, we observe that $\eta_H \approx \widetilde{\eta}_H$ and $\mu_H \approx \widetilde{\mu}_H$ in the sense that the curves almost coincide. For adaptive mesh-refinement, we see furthermore that the error $|||\phi-\phi_h|||$ is accurately estimated by η_H. To exploit these observations in more detail, Figure 4 provides the experimental constants C_{rel}, C_η, and C_μ for the three estimates

$$\eta_H \le |||\phi - \phi_h||| \le C_{\text{rel}}\,\eta_H, \quad \eta_H \le \widetilde{\eta}_H \le C_\eta\,\eta_H, \quad \widetilde{\mu}_H \le \mu_H \le C_\mu\,\mu_H.$$

We see that the reliability constant satisfies $C_{\text{rel}} \approx 1.29$ for uniform mesh-refinement and that C_{rel} is even improved by adaptive mesh-refinement. Moreover, we observe $C_\eta \approx 1.06$ and $C_\mu \approx 1.03$ for uniform mesh-refinement, where both constants tend to 1 for adaptive mesh-refinement.

The sequence of adaptively generated meshes is shown in Figure 5. As can be expected, we observe a strong refinement of the mesh towards the reentrant corner, where ϕ is singular.

6.2. Symm's Integral Equation with Constant Right-Hand Side. The boundary integral equation

$$V\phi = 1 \tag{6.6}$$

with constant right-hand side is considered for the L-shaped domain Ω of Figure 2. The implementation is done as in the previous Example 6.1, despite the fact that the entries of the load vector simply read $\mathbf{b}_j = |T_j|$, which excludes additional errors due to the approximation of the right-hand side.

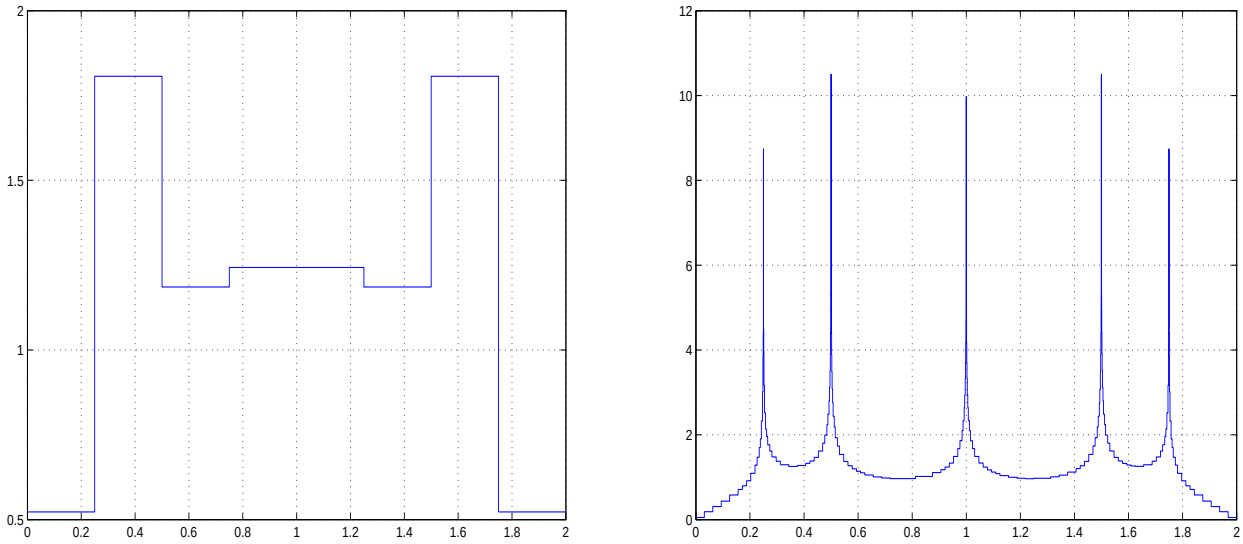

FIGURE 6. Discrete solution $\phi_h^{(0)} \in \mathcal{P}^0(\mathcal{T}_h^{(0)})$ in Capacity Problem 6.2 for the initial mesh $\mathcal{T}_h^{(0)}$ with $N = 8$ elements (left) and $\phi_h^{(9)} \in \mathcal{P}^0(\mathcal{T}_h^{(9)})$ for a $\widetilde{\mu}_H$-adaptively generated mesh $\mathcal{T}_h^{(9)}$ with $N = 180$ elements (right). The figures are plotted over the arclength $s = 0, \dots, 2$, where $s(0) = s(2)$ corresponds to the reentrant corner $(0, 0)$. Note the different scalings of the y-axes, from which singularities at the five convex corners of Ω are visible.

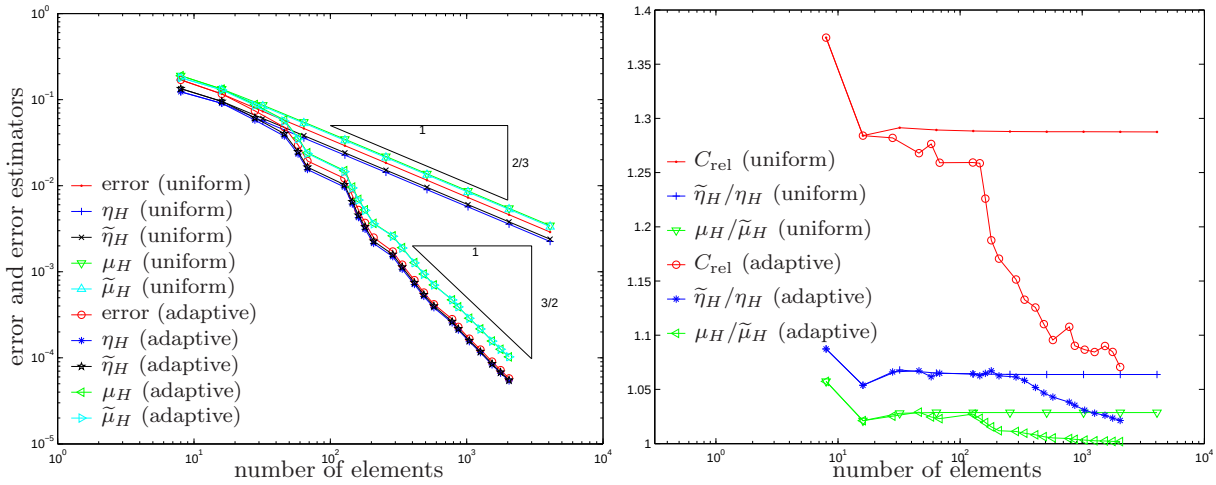

FIGURE 7. Numerical results in Capacity Problem 6.2 on L-shaped domain for uniform and $\widetilde{\mu}_H$-adaptive mesh-refinement: Error $|||\phi - \phi_h|||$ and error estimators η_H, $\widetilde{\eta}_H$, μ_H, $\widetilde{\mu}_H$ (left) and experimental reliability constant $C_{\rm rel} = |||\phi - \phi_h|||/\eta_H$ as well as quotients $\eta_H/\widetilde{\eta}_H$ and $\widetilde{\mu}_H/\mu_H$ (right).

To compute the error in the energy norm, we used the extrapolated value $|||\phi|||^2 = 2.40769127$ in the Galerkin orthogonality (6.5). To the best of our knowledge, the exact solution ϕ is unknown. Figure 6 shows discrete solutions ϕ_h related to the initial mesh and an

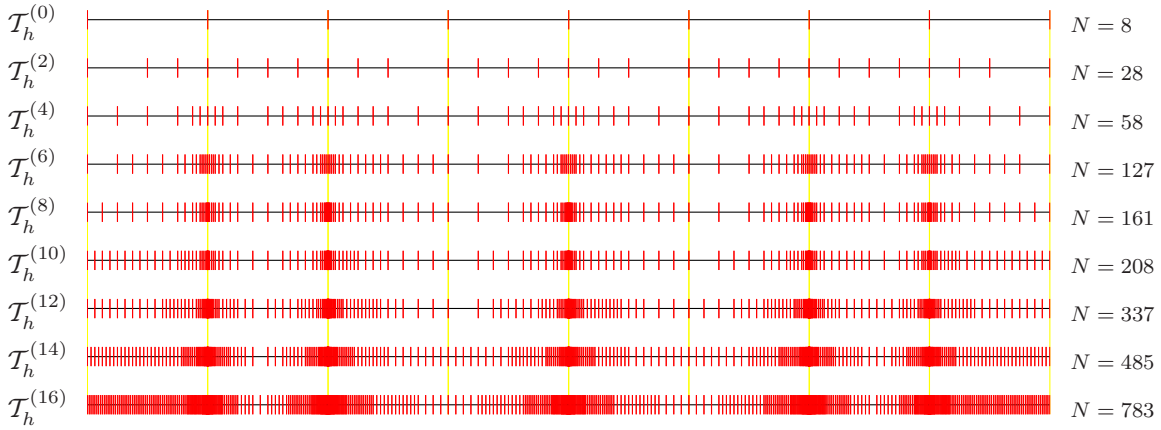

FIGURE 8. $\widetilde{\mu}_H$-adaptively generated meshes in Capacity Problem 6.2 plotted over the arclength $s = 0, \dots, 2$. The mesh-size of the uniform initial mesh $\mathcal{T}_h^{(0)}$ is $h = 1/4$. For the finest mesh $\mathcal{T}_h^{(16)}$ shown, the local mesh-size varies between $h_{\max} = 2^{-6}$ and $h_{\min} = 2^{-18}$. The singularity of ϕ at the five convex corners is reflected by a strong refinement towards the edges at arclength $s = 1/4, 1/2, 1, 3/2, 7/8$.

adaptively generated mesh with $N = 8$ and $N = 180$ elements, respectively. From this plots, the singularities of ϕ at the five convex corners of Γ are clearly visible at arclength $s \in \{1/4, 1/2, 1, 3/2, 7/4\}$. The adaptively generated meshes from Figure 8 show a strong refinement towards these corners.

We stress that we observe the saturation assumption with $q = |||\phi - \phi_{h/2}||| / |||\phi - \phi_h||| < 0.65$ for both mesh-refinement strategies, c.f. Figure 1. Figure 7 shows the error and the four error estimators for uniform and adaptive mesh-refinement. For both mesh-refining strategies, we observe reliability and efficiency of the error estimators. Whereas uniform mesh-refinement leads to suboptimal convergence of order $\mathcal{O}(N^{-2/3})$, adaptive mesh-refinement yields the optimal order $\mathcal{O}(N^{-3/2})$.

For uniform mesh-refinement, we observe $C_{\rm rel} \approx 1.29$, $\eta_H / \widetilde{\eta}_H \approx 1.06$, and $\widetilde{\mu}_H / \mu_H \approx 1.03$. All of these constants are improved for adaptive mesh-refinement. In Figure 7, the curves for η_H and $\widetilde{\eta}_H$ as well as for μ_H and $\widetilde{\mu}_H$ thus appear to coincide.

6.3. Symm's Integral Equation for Exterior Crack Problem. The third example from [ChS] represents a typical end-point singularity for open curves and concerns the Dirichlet problem from Equation (6.1) exterior to a straight slit $\Gamma := (-1, 1) \times \{0\}$, $\Omega := \mathbb{R}^2 \backslash \Gamma$. For $g(x, 0) := -x$, the exact solution ϕ of the corresponding Symm's integral equation reads

$$\phi(x, 0) = -x / \sqrt{1 - x^2} \quad \text{for} \quad -1 < x < 1. \tag{6.7}$$

There holds $\phi \in \widetilde{H}^{-\alpha}(\Gamma)$ for all $\alpha > 0$, but $\phi \notin L^2(\Gamma)$ according to the singularities of ϕ at the tips $\pm(1, 0)$ of Γ. Since Kg vanishes on the straight slit Γ, Symm's integral equation (6.3) simplifies to

$$V\phi = g \quad \text{on } \Gamma. \tag{6.8}$$

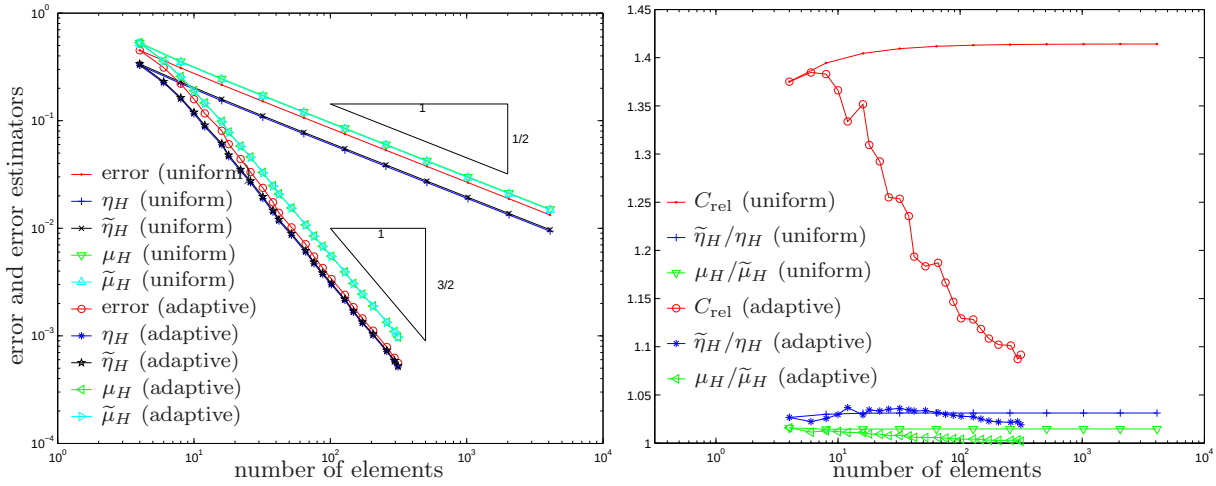

FIGURE 9. Numerical results for the Slit Problem 6.3 on $\Gamma = (-1,1) \times \{0\}$ for uniform and $\widetilde{\mu}_H$-adaptive mesh-refinement: Error $|||\phi - \phi_h|||$ and error estimators η_H, $\widetilde{\eta}_H$, μ_H, $\widetilde{\mu}_H$ (left) and experimental reliability constant $C_{\rm rel} = |||\phi - \phi_h|||/\eta_H$ as well as quotients $\eta_H/\widetilde{\eta}_H$ and $\widetilde{\mu}_H/\mu_H$ (right).

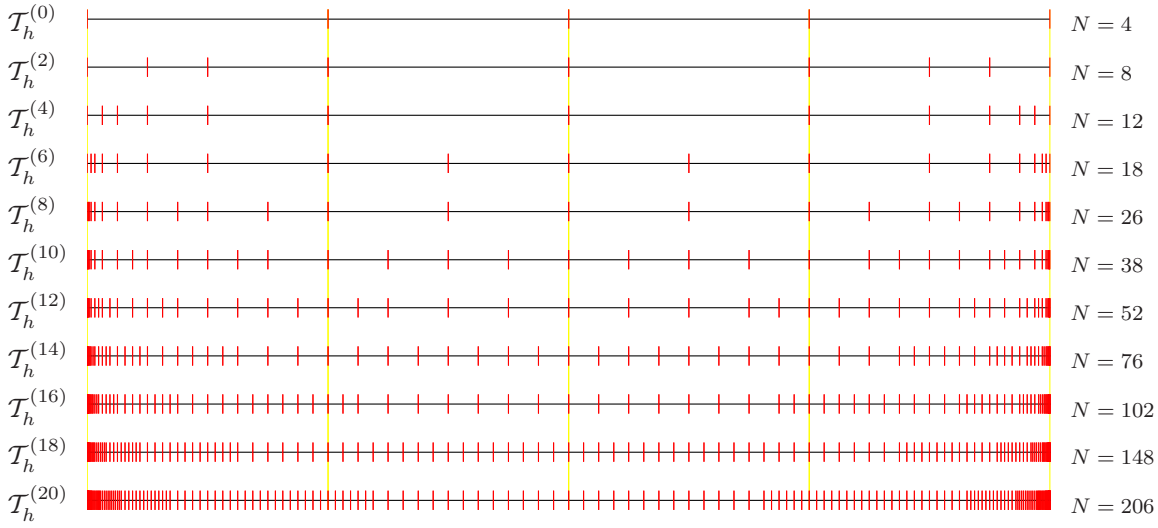

FIGURE 10. $\widetilde{\mu}_H$-adaptively generated meshes in Slit Problem 6.3 plotted over the arclength $s = 0, \dots, 2$. The mesh-size of the uniform initial mesh $\mathcal{T}_h^{(0)}$ is $h = 1/2$. For the finest mesh $\mathcal{T}_h^{(20)}$ shown, the local mesh-size varies between $h_{\max} = 2^{-5}$ and $h_{\min} = 2^{-21}$.

The energy norm of the exact solution can be computed exactly,

$$|||\phi|||^2 = \langle V\phi, \phi \rangle = \int_{-1}^{1} \frac{x^2}{\sqrt{1-x^2}}\, dx = \frac{\pi}{2}.$$

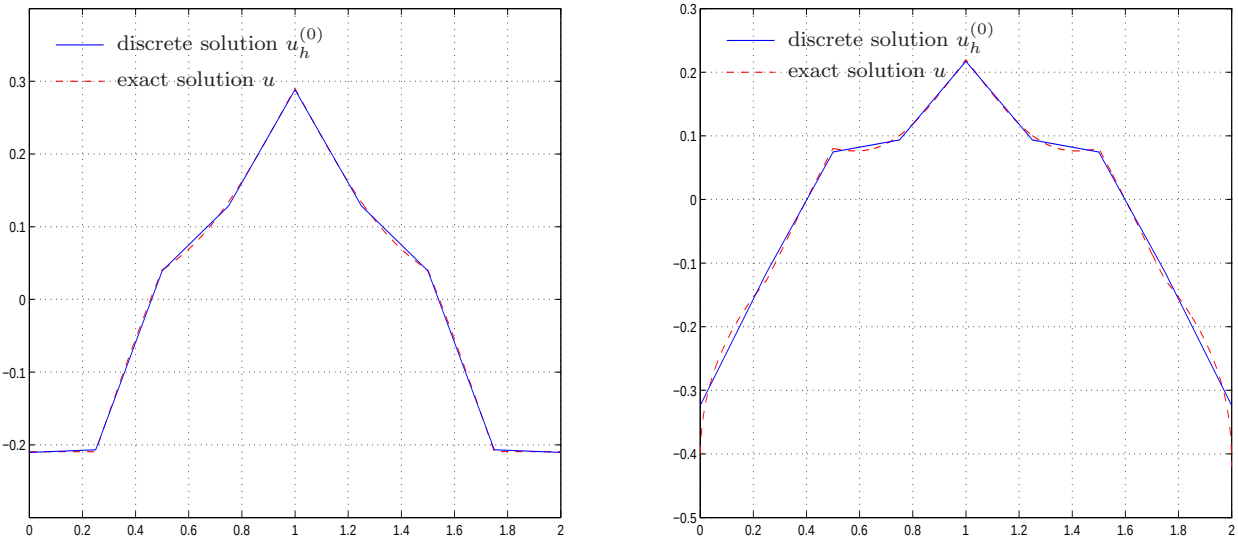

FIGURE 11. Discrete solutions $u_h^{(0)} \in \mathcal{P}^0(\mathcal{T}_h^{(0)})$ in Neumann Problem 6.4 (left) and 6.5 (right) for the initial mesh $\mathcal{T}_h^{(0)}$ with $N = 8$ elements shown in Figure 2. The figures are plotted over the arclength $s = 0, \dots, 2$, where $s(0) = s(2)$ corresponds to the reentrant corner $(0, 0)$. For comparison, we even plot the exact solutions u into both figures. Note that the exact solution of Example 6.4 appears to be piecewise smooth, whereas the exact solution of Example 6.5 has a singularity at the reentrant corner.

For both, uniform and adaptive mesh-refinement, we observe the saturation assumption with experimental constant $q = |||\phi - \phi_{h/2}||| / |||\phi - \phi_h||| < 0.75$. In particular, the error estimators are expected to be reliable and efficient.

Due to the regularity of ϕ, theory predicts a suboptimal convergence of order $\mathcal{O}(N^{-1/2})$ in case of uniform mesh-refinement. This is in fact observed in Figure 9, where we plot the curves of the error and the error estimators for uniform and adaptive mesh-refinement. For both strategies, we again observe reliability and efficiency, and η_H and $\widetilde{\eta}_H$ as well as μ_H and $\widetilde{\mu}_H$ coincide. For uniform mesh-refinement, we observe $C_{\text{rel}} \approx 1.41$, $\eta_H / \widetilde{\eta}_H \approx 1.03$, and $\widetilde{\mu}_H / \mu_H \approx 1.01$. For adaptive-mesh refinement, all of the three quotients improve with the number of elements. In particular, the reliability constant tends down to $C_{\text{rel}} \approx 1.1$ and thus the accuracy of the error estimation improves with the number of elements.

6.4. Hypersingular Integral Equation for Neumann Problem on L-Shaped Domain. We consider a Neumann problem

$$-\Delta U = 0 \text{ in } \Omega \quad \text{with boundary conditions} \quad \partial U / \partial n = g \quad \text{on } \Gamma := \partial\Omega \tag{6.9}$$

with the normal derivative $\partial U / \partial n$, where n denotes the outer unit normal vector on $\partial\Omega$. This problem is equivalent to the hypersingular integral equation

$$W u = (1/2 - K')g \tag{6.10}$$

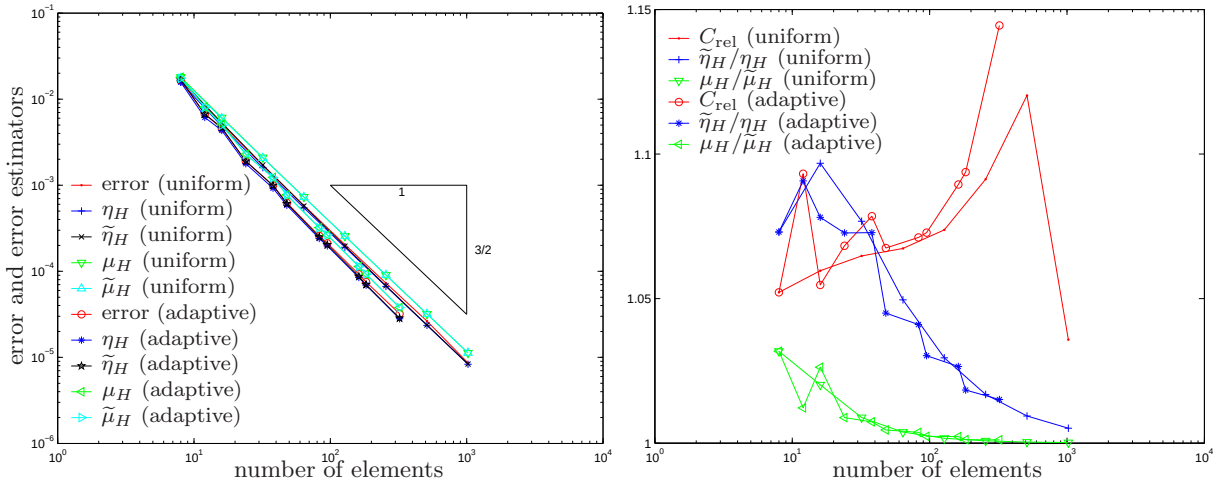

FIGURE 12. Numerical results in Neumann Problem 6.4 on L-shaped domain for uniform and $\widetilde{\mu}_H$-adaptive mesh-refinement: Error $|||u-u_h|||$ and error estimators η_H, $\widetilde{\eta}_H$, μ_H, $\widetilde{\mu}_H$ (left) and experimental reliability constant $C_{\rm rel} = |||u-u_h|||/\eta_H$ as well as quotients $\eta_H/\widetilde{\eta}_H$ and $\widetilde{\mu}_H/\mu_H$ (right).

with the adjoint double-layer potential operator K' from (5.5), c.f. [McL]. Up to an additive constant, the exact solution of (6.10) are just the Dirichlet data $U|_\Gamma$ of U on the boundary Γ. More precisely, there holds $u = U|_\Gamma - \langle U|_\Gamma\,,1\rangle/\langle 1\,,1\rangle$.

For the implementation, we use the nodal basis $\{\psi_1,\dots,\psi_N\}$ of $\mathcal{S}^1(\mathcal{T}_h)$, which consists of the usual hat functions ψ_j. The side constraint $\langle u_h\,,1\rangle = 0$ of the Galerkin solution u_h is realized by a Lagrange multiplier ansatz [CS]. Altogether, the entries of the Galerkin matrix $\mathbf{A} \in \mathbb{R}^{(N+1)\times(N+1)}_{sym}$ read

$$\mathbf{A}_{jk} = \langle W\psi_j\,,\psi_k\rangle \quad\text{and}\quad \mathbf{A}_{j,N+1} = \mathbf{A}_{N+1,j} = \langle \psi_j\,,1\rangle \quad \text{for } j,k = 1,\dots,N, \tag{6.11}$$

and the entries of the load vector $\mathbf{b} \in \mathbb{R}^{N+1}$ are given by

$$\mathbf{b}_j = \langle (1/2 - K')\phi\,,\psi_j\rangle \quad \text{for } j = 1,\dots,N \quad\text{and}\quad \mathbf{b}_{N+1} = 0. \tag{6.12}$$

Then, the Galerkin solution reads $u_h = \sum_{j=1}^N \mathbf{x}_j\psi_j$, where the coefficients are the first N components of the solution $\mathbf{x} \in \mathbb{R}^{N+1}$ of the linear system $\mathbf{A}\mathbf{x} = \mathbf{b}$. Note that in fact $\langle u_h\,,1\rangle = \sum_{j=1}^N \mathbf{x}_j\langle\phi_j\,,1\rangle = (\mathbf{A}\mathbf{x})_{N+1} = b_{N+1} = 0$, and $\mathbf{x}_{N+1}$ is the associated Lagrange multiplier for this side constraint.

The computation of $\mathbf{A}_{jk} = \langle W\psi_j\,,\psi_k\rangle$ is done analytically by use of Nédélec's equation

$$\langle Wu\,,v\rangle = \langle Vu'\,,v'\rangle \quad \text{for all } u,v \in \mathcal{H}^1(\Gamma). \tag{6.13}$$

Here, $(\cdot)' = \partial/\partial s$ denotes the arclength derivative. Moreover, for the implementation of the Galerkin scheme we do not evaluate the right-hand side in the form of Equation (6.10). Instead, we use that in Example 6.4 and 6.5 the exact solution u is known and compute $\langle(1/2-K')\phi\,,\psi_j\rangle = \langle Wu\,,\psi_j\rangle = \langle W\psi_j\,,u\rangle$ by use of (6.13). Here, the integrand $u'(x)V\psi_j'(x)$ which appears in the computation of the load vector, may have logarithmic singularities. We used an h-adaptive Simpson formula and Romberg extrapolation down to a tolerance 10^{-12} for each occurring integral.

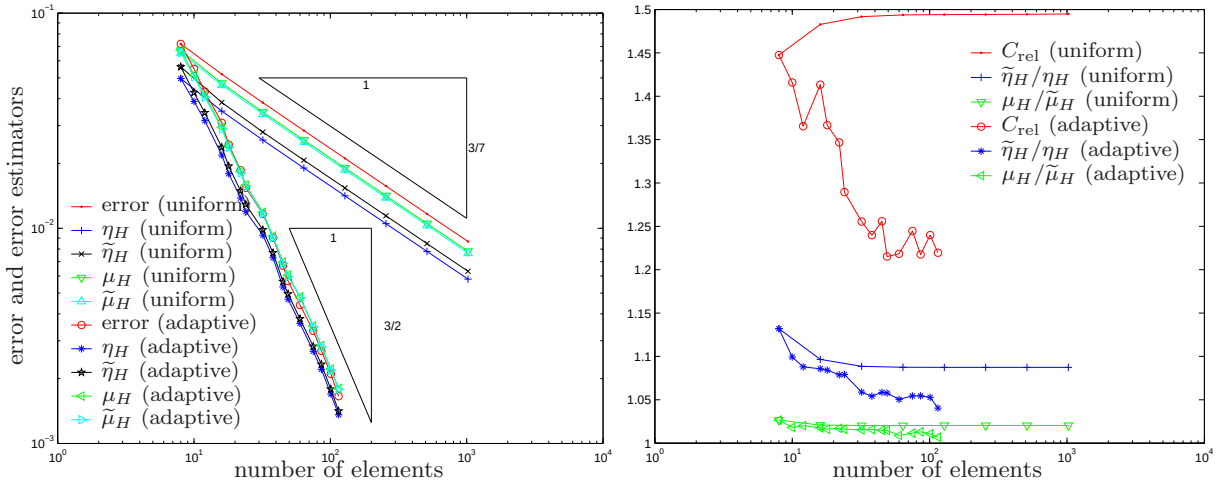

FIGURE 13. Numerical results in Neumann Problem 6.5 on L-shaped domain for uniform and $\widetilde{\mu}_H$-adaptive mesh-refinement: Error $|||u-u_h|||$ and error estimators η_H, $\widetilde{\eta}_H$, μ_H, $\widetilde{\mu}_H$ (left) and experimental reliability constant $C_{\rm rel} = |||u-u_h|||/\eta_H$ as well as quotients $\eta_H/\widetilde{\eta}_H$ and $\widetilde{\mu}_H/\mu_H$ (right).

For our first numerical experiment, we consider the Neumann problem (6.9) on the L-shaped domain Ω from Figure 2 with given exact solution U from (6.2) with $\alpha = 2/3$. As for Symm's integral equation, the error in the energy norm is computed with the help of the Galerkin orthogonality

$$|||u-u_h||| = \big(|||u|||^2 - |||u_h|||^2\big)^{1/2}. \tag{6.14}$$

The extrapolated energy $|||u|||^2 = 0.1742589574$ is obtained by Aitkin's Δ^2 method. The solution u is plotted over the arclength in Figure 11. In particular, we observe that u appears to be piecewise smooth, which corresponds to the fact that the experimental saturation constant $q < 0.55$ is rather small, c.f. Figure 1.

We consider the four introduced error estimators

$$\eta_H = |||u_{h/2} - u_h|||, \qquad \mu_H = \|h^{1/2}(u_{h/2}-u_h)'\|_{L^2(\Gamma)},$$
$$\widetilde{\eta}_H = |||u_{h/2} - I_h u_{h/2}|||, \qquad \widetilde{\mu}_H = \|h^{1/2}(u_{h/2}-I_h u_{h/2})'\|_{L^2(\Gamma)},$$

where I_h denotes the nodal interpolation operator. According to Theorem 4.4, there holds

$$\eta_H \le \widetilde{\eta}_H \lesssim \widetilde{\mu}_H \le \mu_H \lesssim \eta_H,$$

i.e. all error estimators are equivalent. We have efficiency of η_H, and hence of all estimators, with constant $C_{\rm eff} = 1$ for η_H. Reliability of the four estimators depends on the saturation assumption and is empirically observed throughout.

Figure 12 shows the numerical results for uniform and adaptive mesh-refinement. As may be expected from the plot of the exact solution in Figure 11, uniform mesh-refinement leads to the optimal order $\mathcal{O}(N^{-3/2})$ of convergence. However, we even see that adaptive mesh-refinement yields improved results in the following sense: The curve of the error with respect to adaptive mesh-refinement is a lower parallel of the corresponding curve for uniform mesh-refinement. This means that the absolute values of the error for a fixed number of elements

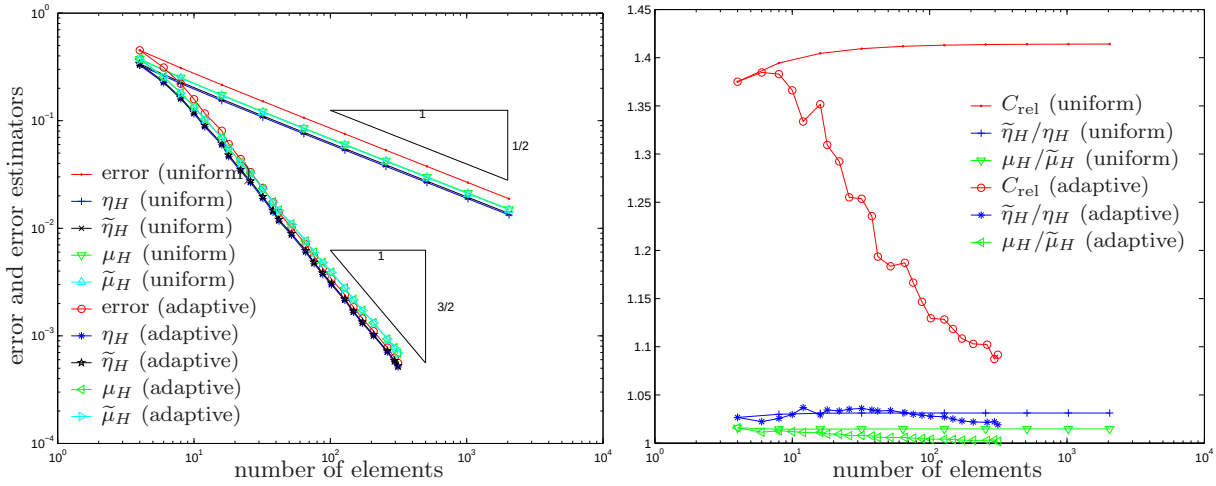

FIGURE 14. Numerical results in Example 6.6 on the slit $(-1,1)\times\{0\}$ for uniform and $\widetilde{\mu}_H$-adaptive mesh-refinement: Error $|||u-u_h|||$ and error estimators η_H, $\widetilde{\eta}_H$, μ_H, $\widetilde{\mu}_H$ (left) and experimental reliability constant $C_{\rm rel} = |||u-u_h|||/\eta_H$ as well as quotients $\eta_H/\widetilde{\eta}_H$ and $\widetilde{\mu}_H/\mu_H$ (right).

are improved by the adaptive scheme. Moreover, the curves in Figure 12 show that the error estimators η_H and $\widetilde{\eta}_H$ as well as μ_H and $\widetilde{\mu}_H$ coincide, where the quotients $\eta_H/\widetilde{\eta}_H$ as well as $\mu_H/\widetilde{\mu}_H$ tend to 1 with the increasing number of elements. The error estimation is very accurate in the sense that the curves of η_H and the error $|||u-u_h|||$ almost coincide up to a constant $C_{\rm rel}\le 1.15$ in the range of the computation.

6.5. Hypersingular Integral Equation on L-Shaped Domain with Singular Solution. We consider the same example as in Neumann Problem 6.4 but now with parameter $\alpha = 3/7$. The exact solution u of the hypersingular integral equation then shows a singularity at the reentrant corner, c.f. Figure 11. The experimental saturation constant satisfies $q = |||u-u_{h/2}|||/|||u-u_h||| < 0.75$, c.f. Figure 1.

For the computation of the error in the energy norm, we used the extrapolated energy $|||u|||^2 = 0.1560404049$ in (6.14). Figure 13 then shows error and error estimators for uniform and adaptive mesh-refinement. The uniform mesh-refinement leads to a suboptimal experimental convergence rate of order $\mathcal{O}(N^{-3/7})$ for the error. Adaptive mesh-refinement retains the optimal order of convergence $\mathcal{O}(N^{-3/2})$. As expected from the experimental saturation constant, all error estimators are observed to be reliable and efficient. For uniform mesh-refinement, we obtain $C_{\rm rel}\approx 1.49$, $\eta_H/\widetilde{\eta}_H\approx 1.09$, and $\widetilde{\mu}_H/\mu_H\approx 1.02$. Again, these values are improved for the adaptive strategy.

6.6. Hypersingular Integral Equation on a Straight Slit. Our last example for the hypersingular integral equation is concerned with

$$Wu = 1 \quad \text{on the slit } \Gamma = (-1,1)\times\{0\}. \tag{6.15}$$

The exact solution $u\in\widetilde{H}^{1/2}(\Gamma)$ is given by

$$u(x,0) = \sqrt{1-x^2} \quad \text{for } -1<x<1.$$

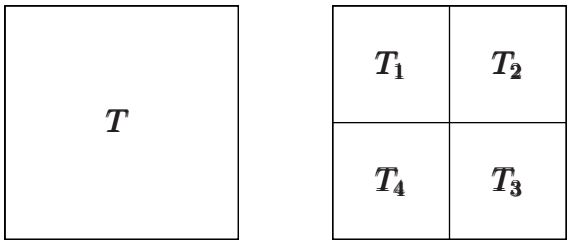

FIGURE 15. A marked element T is always refined uniformly into 4 new elements T_j. This refinement obviously yields $h_j = h/2$ and $\varrho_j = \varrho/2$ for the refined mesh-sizes.

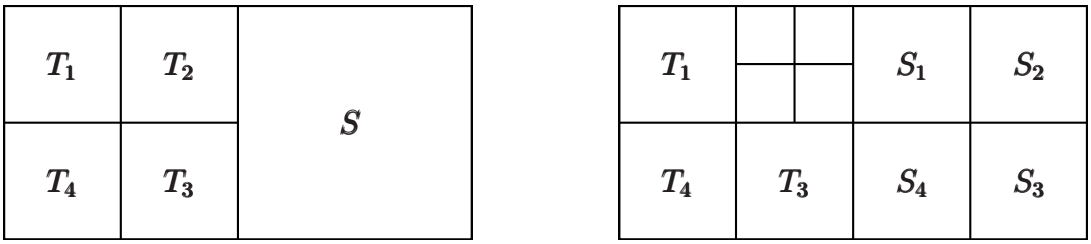

FIGURE 16. One hanging node per edge is allowed (left). If, in the left configuration, element T_2 is marked for refinement, we mark element S for refinement as well (right).

There holds $u \in H^{1-\varepsilon}(\Gamma)$ for all $\varepsilon > 0$, but $u \notin H^1(\Gamma)$. Note that there is a strong connection with Example 6.3 in the sense that $u'(x,0) = -\frac{x}{\sqrt{1-x^2}} = \phi(x,0)$ for the arc-length derivative $(\cdot)' = \partial/\partial s$ and $\phi \in \widetilde{H}^{-1/2}(\Gamma)$ the exact solution of Example 6.3. In particular, the exact energy reads

$$|||u|||^2 = \langle Wu\,,u\rangle = \langle V\phi\,,\phi\rangle = \pi/2$$

according to Nédélec's equation (6.13). Moreover, with $g(x,0) = -x$ the right-hand side in Example 6.3, any Galerkin approximation $u_h \in \mathcal{S}^1_0(\mathcal{T}_h)$ of u satisfies

$$\langle Vu_h'\,,v_h'\rangle = \langle Wu_h\,,v_h\rangle = \langle 1\,,v_h\rangle = \langle g\,,v_h'\rangle \quad \text{for all } v_h \in \mathcal{S}^1_0(\mathcal{T}_h).$$

Therefore, the corresponding arc-length derivative u_h' is the Galerkin approximation of ϕ with respect to the discrete space $\mathcal{P}^0_0(\mathcal{T}_h) := \{\psi_h \in \mathcal{P}^0(\mathcal{T}_h) : \int_\Gamma \psi_h\,ds = 0\}$. Since ϕ satisfies $\int_\Gamma \phi\,ds = 0$, it comes as no surprise that the overall numerical results of Example 6.6 almost coincide with the results of Example 6.3, c.f. Figure 9 and 14 for details, respectively.

7. Numerical Experiments in 3D with Isotropic Mesh-Refinement

In this and the following section, we study the performance of the proposed method for Symm's integral equation in 3D. For the ease of implementation and to exclude any positive

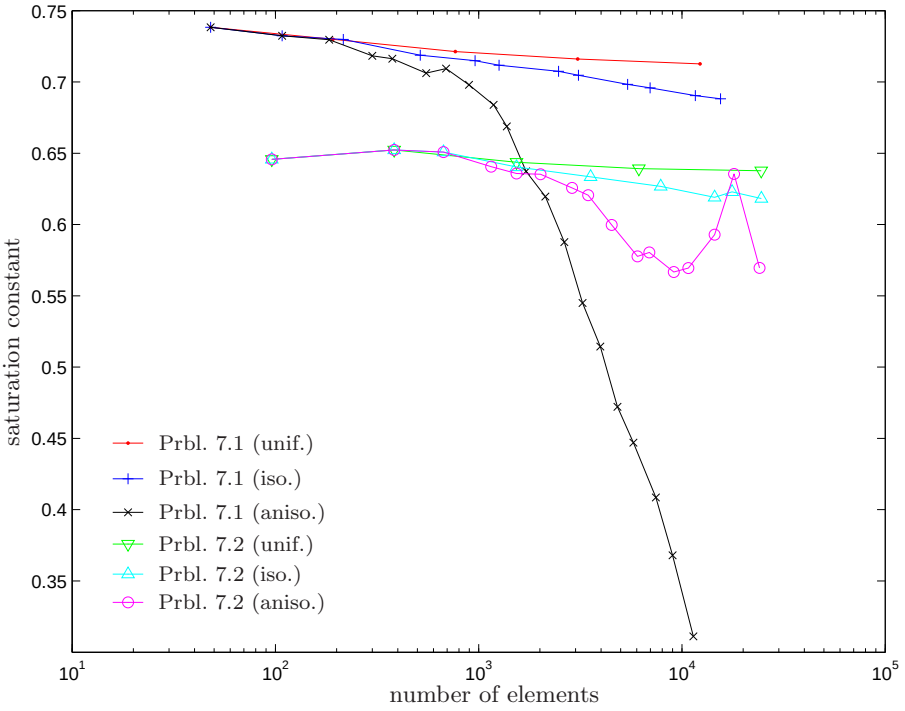

FIGURE 17. Experimental saturation constant $q = |||\phi - \phi_{h/2}|||/|||\phi - \phi_h|||$ for Screen Problem 7.1 and Capacity Problem 7.2 for uniform as well as $\widetilde{\mu}_H$-adaptive isotropic and anisotropic mesh-refinement. In any case holds $q \leq 0.75$, which yields reliability of η_H.

or negative effects of numerical quadrature, we consider

$$V\phi = 1 \quad \text{on } \Gamma, \tag{7.1}$$

for Γ being the L-shaped screen in Example 7.1 and the surface $\Gamma = \partial\Omega$ of the reference cube $\Omega = (-1,1)^3$ in Example 7.2. In both cases, the solution ϕ appears to be singular so that uniform mesh-refinement leads to a suboptimal order of convergence for the error $|||\phi - \phi_h|||$. Although this is improved by adaptive isotropic mesh-refinement, we do not reveal the optimal order of convergence. In Section 8 below, we thus develop an adaptive strategy for anisotropic mesh-refinement, which finally leads to the optimal results.

The saturation constant $q = |||\phi - \phi_{h/2}|||/|||\phi - \phi_h|||$ is visualized in Figure 17 for all three mesh-refinement strategies, namely uniform as well as $\widetilde{\mu}_H$-adaptive isotropic and $\widetilde{\mu}_H$-adaptive anisotropic mesh-refinement, respectively. In any case and for both examples, we see that q is uniformly bounded by 0.75, which empirically proves the reliability of η_H.

7.1. Symm's Integral Equation on L-Shaped Screen. We consider Symm's integral equation (7.1) on the L-shaped screen Γ, which is visualized together with the uniform initial mesh $\mathcal{T}_h^{(0)}$ in Figure 18. The exact solution ϕ is unknown, but discrete solutions show certain singularities along the edges and at the five convex corners of Γ.

The implementation follows along the lines of the 2D case, c.f. Section 6.1 above. Throughout, we restrict to the case that the elements $T_j \in \mathcal{T}_h$ are axis parallel rectangles so that all entries of the Galerkin matrix can be computed analytically [M]. As in the 2D examples

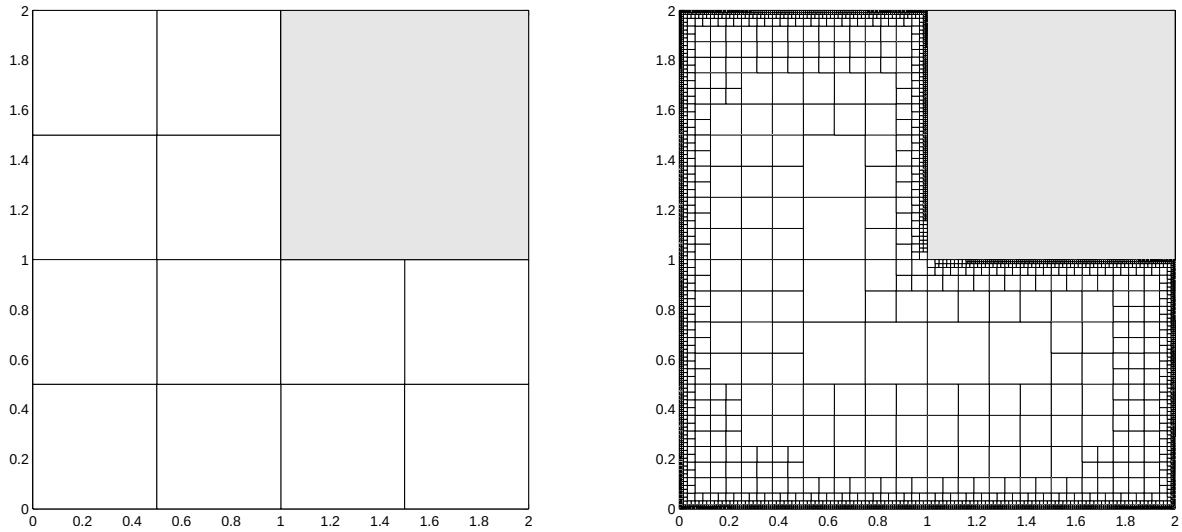

FIGURE 18. Initial mesh $\mathcal{T}_h^{(0)}$ with $N = 12$ elements (left) in Screen Problem 7.1 as well as mesh $\mathcal{T}_h^{(11)}$ with $N = 3870$ elements obtained by $\widetilde{\mu}_H$-adaptive isotropic mesh-refinement (right). For the adaptively generated mesh $\mathcal{T}_h^{(11)}$, we observe mesh-refinement along the edges of Γ.

above, all computations are performed by Algorithm 3.3 with $\theta = 0$ for uniform and $\theta = 0.5$ for adaptive mesh-refinement. For the marking in step (v) of Algorithm 3.3, we again use the localized error estimator $\widetilde{\mu}_H$. For the isotropic refinement, each marked element T_j is split into 4 new elements such that h_j as well as ϱ_j are halved, c.f. Figure 15. We stress that, due to the initial mesh and our isotropic mesh-refinement rule, the mesh-widths $\varrho = h$ coincide. To ensure the K-mesh property of the triangulations, we only allow one hanging node per edge, c.f. Figure 16.

To compute the error in the energy norm, we use the extrapolated value $|||\phi|||^2 = 8.28457059$ obtained from Aitkin's Δ^2-method. Besides the error, we consider the four error estimators

$$\eta_H = |||\phi_{h/2} - \phi_h|||, \qquad \mu_H = \|h^{1/2}(\phi_{h/2} - \phi_h)\|_{L^2(\Gamma)},$$
$$\widetilde{\eta}_H = |||\phi_{h/2} - \Pi_h\phi_{h/2}|||, \qquad \widetilde{\mu}_H = \|h^{1/2}(\phi_{h/2} - \Pi_h\phi_{h/2})\|_{L^2(\Gamma)},$$

where Π_h denotes the L^2-projection onto $\mathcal{P}^0(\mathcal{T}_h)$.

Error and error estimators are plotted in Figure 19 over the number $N = \#\mathcal{T}_h$ of elements. As predicted by theory, all error estimators are efficient, and the corresponding curves are parallel since there holds the equivalence inequality

$$\eta_H \le \widetilde{\eta}_H \lesssim \widetilde{\mu}_H \le \mu_H \lesssim \eta_H.$$

Moreover, for both mesh-refining strategies, we obtain experimental reliability since the curve of the error $|||\phi - \phi_h|||$ is parallel to the curves of the corresponding error estimators. We observe a certain deviation of μ_H and $\widetilde{\mu}_H$ resp. η_H and $\widetilde{\eta}_H$, which is visualized in terms of the quotients $\widetilde{\eta}_H/\eta_H$ and $\mu_H/\widetilde{\mu}_H$ in Figure 20: Both strategies, uniform and isotropic refinement, lead to basically the same relations $\widetilde{\eta}_H/\eta_H \approx 1.3$ and $\mu_H/\widetilde{\mu}_H \approx 1.01$. The constant $C_{\rm rel} = |||\phi - \phi_H|||/\eta_H$ tends to become slightly better, meaning closer to 1, with

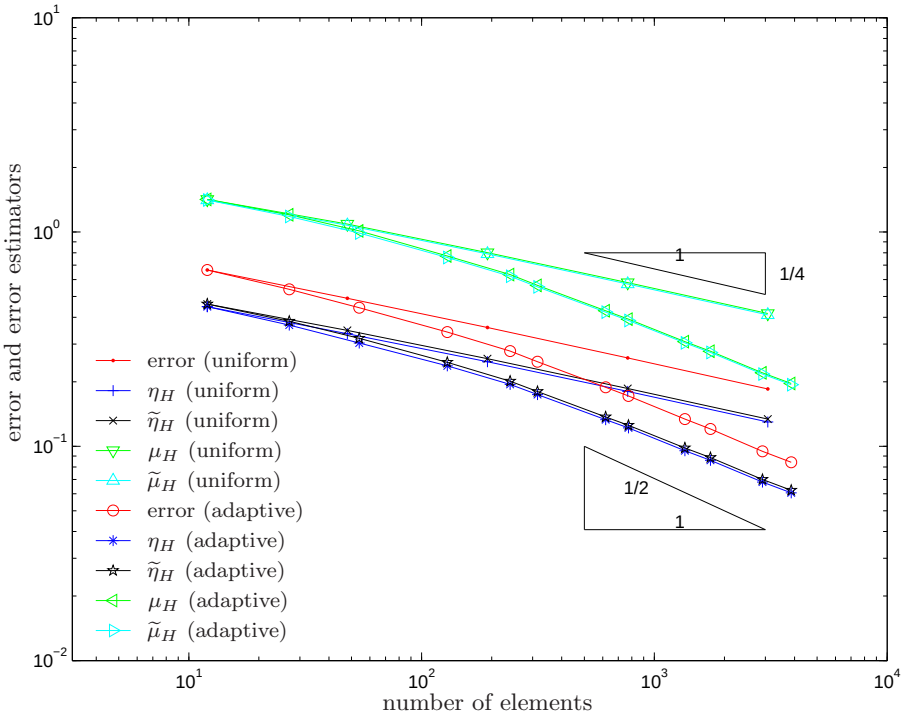

FIGURE 19. Error $|||\phi - \phi_h|||$ and error estimators $\eta_H, \widetilde{\eta}_H, \mu_H, \widetilde{\mu}_H$ in Screen Problem 7.1 for uniform and $\widetilde{\mu}_H$-adaptive isotropic mesh-refinement.

isotropic mesh-refinement. With respect to the order of convergence, we observe that uniform refinement leads to a suboptimal order $\mathcal{O}(N^{-1/4})$ which corresponds to $\mathcal{O}(h^{1/2})$ in terms of the uniform mesh-size h. The $\widetilde{\mu}_H$-adaptive strategy leads to an improved convergence order of almost $\mathcal{O}(N^{-1/2})$. However, the optimal order of convergence is $\mathcal{O}(N^{-3/4})$ so that the adaptive isotropic mesh-refinement is far from being optimal.

7.2. Capacity Problem on Reference Cube. Again, we consider Symm's integral equation (7.1), this time on the boundary Γ of the reference cube $\Omega = (-1,1)^3$. The exact solution ϕ is unknown. The initial mesh $\mathcal{T}_h^{(0)}$ is shown in Figure 21 and consists of $N = 24$ uniform square elements with edge length 1.

We use the extrapolated value $|||\phi|||^2 = 16.6047032$ in (6.5) to compute the error $|||\phi - \phi_h|||$. The error and the four estimators are plotted in Figure 22. As in Example 7.1, we observe that the convergence order is improved from $\mathcal{O}(N^{-1/4})$ to $\mathcal{O}(N^{-1/2})$ in case of $\widetilde{\mu}_H$-adaptive isotropic refinement. Independently of both mesh-refining strategies, all error estimators are empirically proven to be efficient and reliable. The experimental reliability is reflected in the boundedness $q = |||\phi - \phi_{h/2}|||/|||\phi - \phi_h||| \leq 0.7$ of the saturation constant shown in Figure 17.

As in the previous example, we have a certain deviation of η_H and $\widetilde{\eta}_H$ resp. μ_H and $\widetilde{\mu}_H$. We observe $\widetilde{\eta}_H/\eta_H \approx 1.06$ and $\mu_H/\widetilde{\mu}_H \approx 1.03$ which seems to hold for both strategies. The experimental reliability constant reads $C_{\mathrm{rel}} = |||\phi - \phi_h|||/\eta_H \approx 1.30$ for uniform mesh-refinement and is slightly improved for adaptive mesh-refinement. A plot of these constants can be seen in Figure 23.

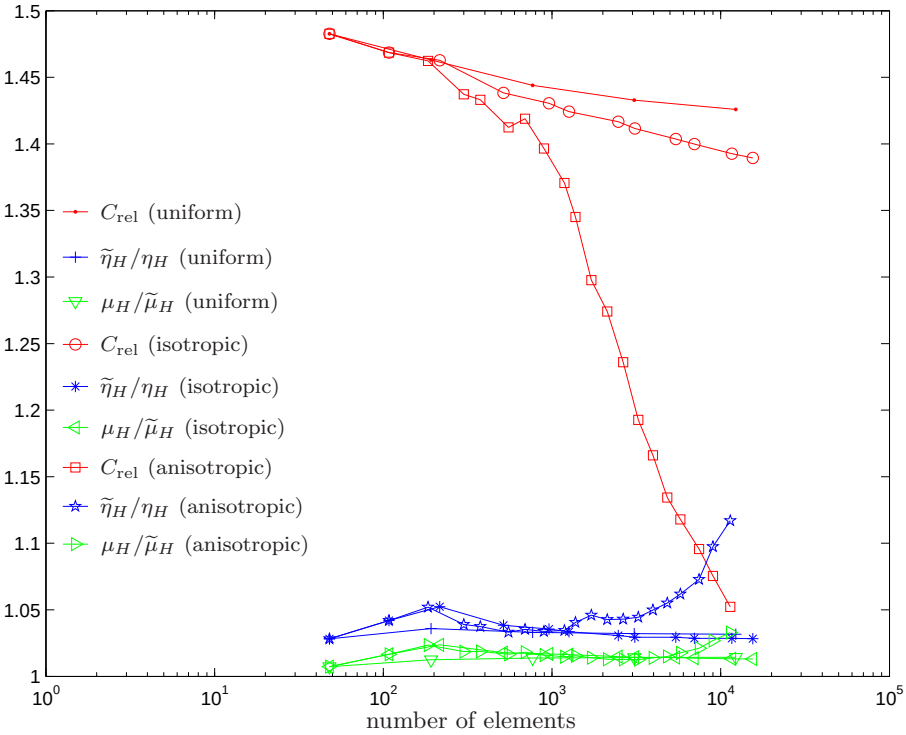

FIGURE 20. Experimental reliability constant $C_{\rm rel} = |||\phi - \phi_h|||/\eta_H$ as well as quotients $\eta_H/\widetilde{\eta}_H$ and $\widetilde{\mu}_H/\mu_H$ in Screen Problem 7.1 for uniform as well as $\widetilde{\mu}_H$-adaptive isotropic and anisotropic mesh-refinement.

8. Numerical Experiments in 3D with Anisotropic Mesh-Refinement

In Section 6, we observed that the adaptive Algorithm 3.3 retains the optimal order of convergence for the numerical solution of Symm's integral equation and the hypersingular integral equation in 2D. The experiments in Section 7 revealed that for Symm's integral equation in 3D the experimental order of convergence is improved, when compared to the order of convergence for uniform mesh-refinement. The adaptive isotropic mesh-refinement still leads to a suboptimal order of convergence. To overcome this gap, we extend Algorithm 3.3 to allow anisotropic mesh-refinement. We stress, however, that the new algorithm is not fully covered by theory.

8.1. Adaptive Algorithm for Anisotropic Mesh-Refinement. In the following, we extend step (v) of Algorithm 3.3 by a heuristic criterion to decide whether a marked rectangle $T \in \mathcal{T}_h$ should be refined into 2 or 4 rectangles, c.f. Figure 24. To that end, we use that we have already computed $\phi_{h/2}$. Let $T_1, \dots, T_4 \in \mathcal{T}_{h/2}$ denote the four son-elements of T, where we use the same numbering as for the isotropic refinement of Figure 24. Now, consider the four piecewise constant functions $\psi_{T,j} \in \mathcal{P}^0(\mathcal{T}_{h/2})$ from Figure 25 and observe that $\{\psi_{T,1}, \dots, \psi_{T,4}\}$ is an L^2-orthogonal basis of $\mathcal{P}^0(\{T_1, \dots, T_4\})$. Therefore, $\phi_{h/2}|_T \in$

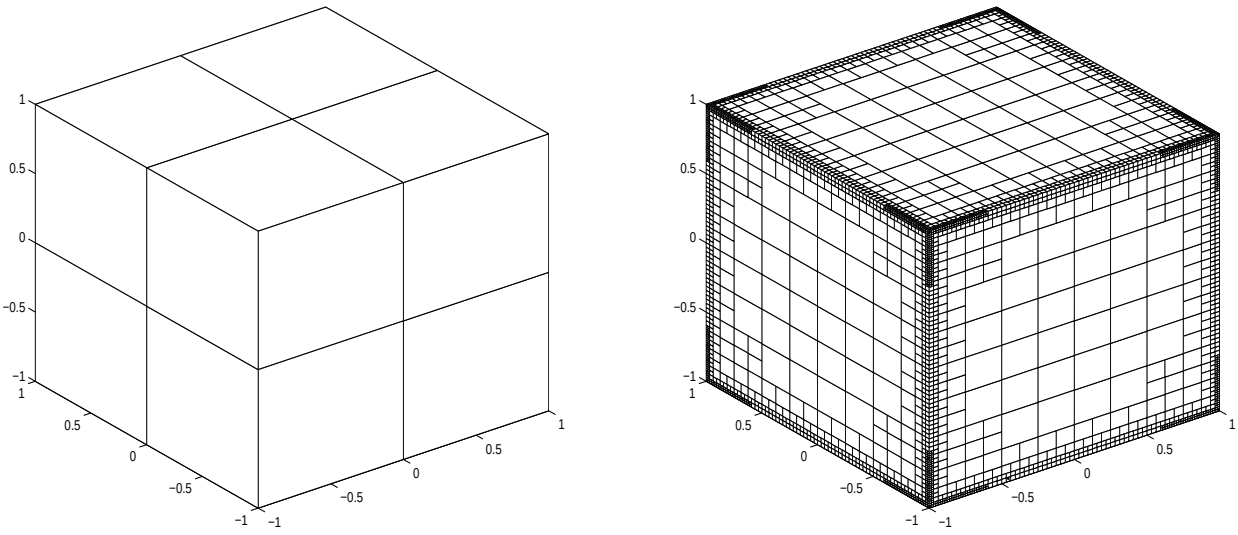

FIGURE 21. Initial mesh $\mathcal{T}_h^{(0)}$ with $N = 24$ Elements (left) in Capacity Problem 7.2 as well as mesh $\mathcal{T}_h^{(8)}$ with $N = 6150$ elements obtained by $\widetilde{\mu}_H$-adaptive isotropic mesh-refinement (right). We observe mesh-refinement along the edges and towards the corners of the cube.

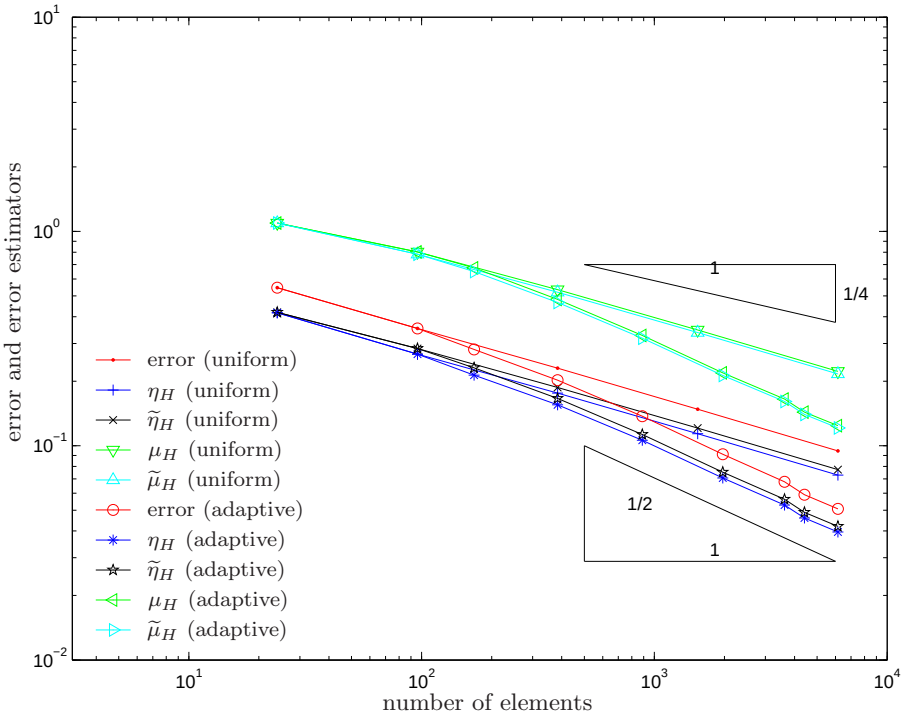

FIGURE 22. Error $|||\phi - \phi_h|||$ and error estimators $\eta_H, \widetilde{\eta}_H, \mu_H, \widetilde{\mu}_H$ in Capacity Problem 7.2 for uniform and $\widetilde{\mu}_H$-adaptive isotropic mesh-refinement.

$\mathcal{P}^0(\{T_1, \ldots, T_4\})$ reads

$$\phi_{h/2}|_T = \sum_{j=1}^{4} c_{T,j}\psi_{T,j} \quad \text{with the Fourier coefficients} \quad c_{T,j} = \frac{(\psi_{T,j}\ , \phi_{h/2})_{L^2(T)}}{\|\psi_{T,j}\|^2_{L^2(T)}}. \tag{8.1}$$

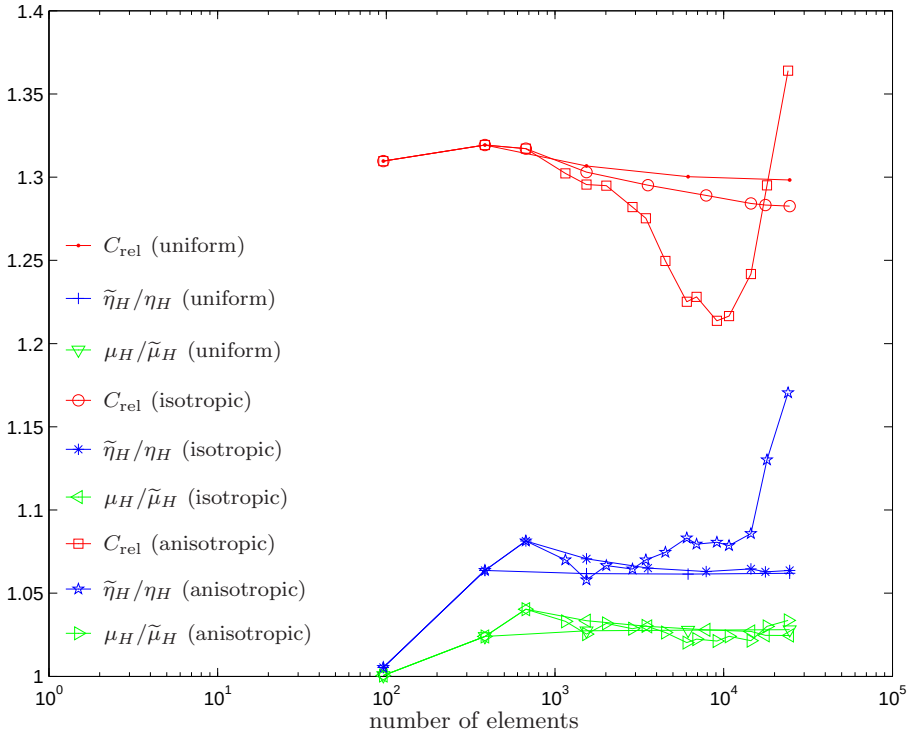

FIGURE 23. Experimental reliability constant $C_{\rm rel} = |||\phi - \phi_h|||/\eta_H$ as well as quotients $\eta_H/\widetilde{\eta}_H$ and $\mu_H/\widetilde{\mu}_H$ in Capacity Problem 7.2 for uniform and $\widetilde{\mu}_H$-adaptive isotropic and anisotropic mesh-refinement.

The decision which refinement is more appropriate, is now done as follows.We assume that $T \in \mathcal{T}_h$ is marked for refinement:

- If $c_{T,3}$ is significantly larger than the Fourier coefficients $c_{T,2}$ and $c_{T,4}$ the discrete solution $\phi_{h/2}|_T$ is rather constant in the horizontal direction. Therefore, the vertical refinement from Figure 24 seems to be more efficient than isotropic refinement.
- If $c_{T,4}$ is significantly larger than the Fourier coefficients $c_{T,2}$ and $c_{T,3}$, the discrete solution $\phi_{h/2}|_T$ is rather constant in the vertical direction. Therefore, the horizontal refinement from Figure 24 seems to be more efficient than isotropic refinement.
- Otherwise, we do isotropic refinement.

Here, significantly larger is understood in the following sense: Let $\tau \in (0,1)$ be a fixed parameter. Then, $c_{T,3}$, for instance, is significantly larger than $c_{T,2}$ and $c_{T,4}$, provided that

$$\tau |c_{T,3}| \geq \left(|c_{T,2}|^2 + |c_{T,4}|^2\right)^{1/2}. \tag{8.2}$$

For the numerical experiments, we choose $\tau = 0.5$.

Finally, we recall that the Fourier coefficients are easy to compute. In our implementation, we use $\mathcal{B} := \{\chi_T : T \in \mathcal{T}_h\}$ as basis of $\mathcal{P}^0(\mathcal{T}_h)$, where χ_T is the characteristic function of $T \in \mathcal{T}_h$. In particular, our computations provide the coefficients $\lambda_{T,1}, \ldots, \lambda_{T,4} \in \mathbb{R}$ such that

$$\phi_{h/2}|_T = \sum_{j=k}^{4} \lambda_{T,k} \chi_{T_k},$$

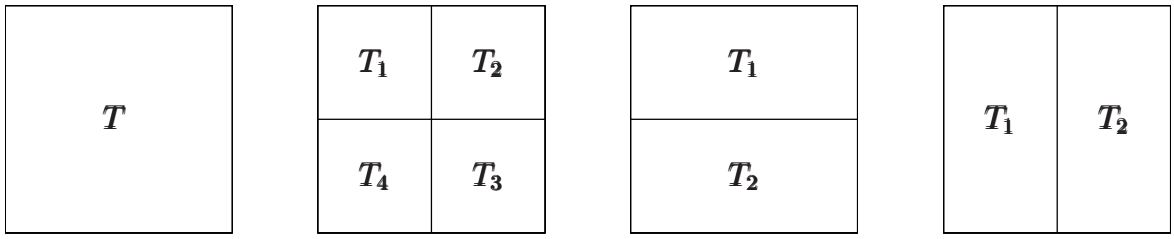

marked element | isotropic refinement | vertical refinement | horizontal refinement

FIGURE 24. The modification of Algorithm 3.3 gives a criterion whether a marked rectangle $T \in \mathcal{T}_h$ (left) is refined isotropically into four elements $T_1, \ldots, T_4$ or anisotropically into two elements T_1 and T_2. In the latter case, the algorithm decides whether vertical or horizontal refinement seems to be more appropriate.

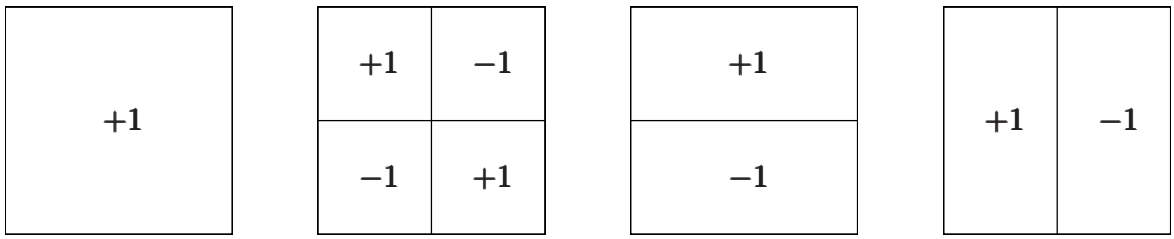

$\psi_{T,1}$ | $\psi_{T,2}$ | $\psi_{T,3}$ | $\psi_{T,4}$

FIGURE 25. For each rectangle $T \in \mathcal{T}_h$ we introduce four $\mathcal{T}_{h/2}$-piecewise constant functions $\psi_{T,j} \in \mathcal{P}^0(\mathcal{T}_{h/2})$, which are extended by zero to $\Gamma \backslash T$.

where $T_1, \ldots, T_4 \in \mathcal{T}_{h/2}$ are the sons of $T \in \mathcal{T}_h$ as in Figure 24. We then observe

$$\|\psi_{T_j}\|^2_{L^2(T)} = |T| \quad \text{as well as} \quad (\psi_{T,j}\,, \phi_{h/2})_{L^2(T)} = \sum_{k=1}^{4} \lambda_{T,k} \int_{T_k} \psi_{T,j}\, dx.$$

Note that the integral has the value $\pm|T|/4$ according to the definition of the functions $\psi_{T,j}$. A comparison of Figure 24 and 25 now shows that

$$\begin{pmatrix} c_{T,1} \\ c_{T,2} \\ c_{T,3} \\ c_{T,4} \end{pmatrix} = \frac{1}{4} \begin{pmatrix} 1 & 1 & 1 & 1 \\ 1 & -1 & 1 & -1 \\ 1 & 1 & -1 & -1 \\ 1 & -1 & -1 & 1 \end{pmatrix} \begin{pmatrix} \lambda_{T,1} \\ \lambda_{T,2} \\ \lambda_{T,3} \\ \lambda_{T,4} \end{pmatrix},$$

where we simply plugged-in the values $\psi_{T,j}|_{T_k}$.

8.2. Numerical Experiments with Anisotropic Mesh-Refinement. To study the performance of the extended algorithm, we consider the Screen Problem 7.1 and the Capacity Problem 7.2. Experimental convergence rates are shown in Figure 27 and Figure 29 for Example 7.1 and Example 7.2, respectively. We plot the error $|||\phi - \phi_h|||$ and the error

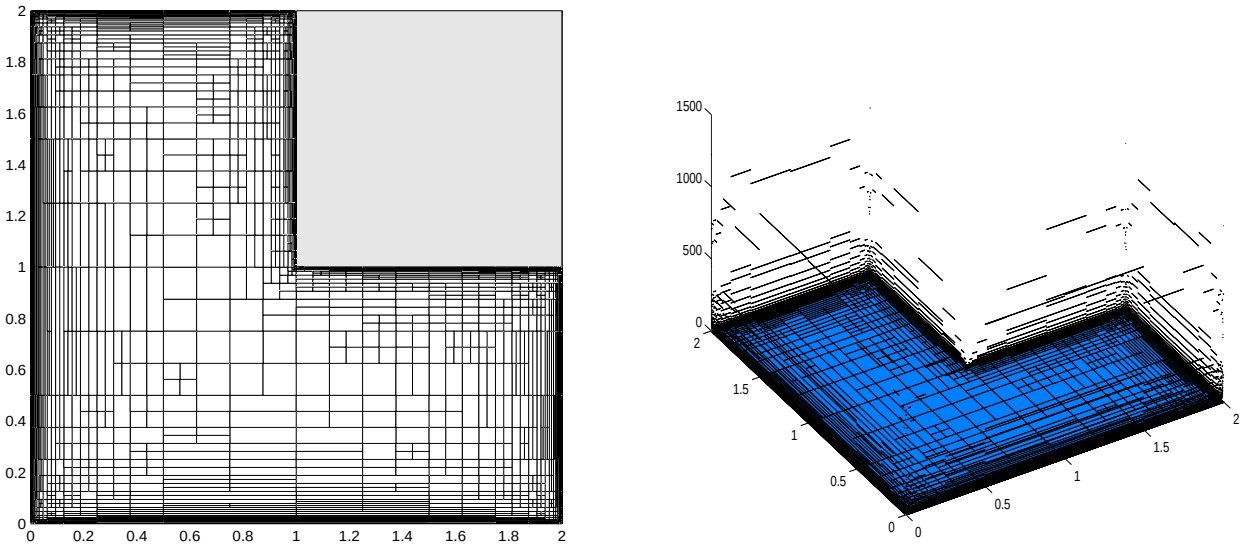

FIGURE 26. Mesh $\mathcal{T}_h^{(19)}$ with $N = 2846$ elements in Screen Problem 7.1 (left) obtained by $\widetilde{\mu}_H$-adaptive anisotropic mesh-refinement. We used the parameters $\theta = 0.5$ in Algorithm 3.3 for marking and $\tau = 0.5$ to decide the type of refinement, cf. Section 8.1. The singularities of the corresponding discrete solution $\phi_h^{(19)}$ along the edges and at all but the reentrant corner are clearly visible (right).

estimators

$$\eta_H = |||\phi_{h/2} - \phi_h|||, \qquad \mu_H = \|\varrho^{1/2}(\phi_{h/2} - \phi_h)\|_{L^2(\Gamma)},$$
$$\widetilde{\eta}_H = |||\phi_{h/2} - \Pi_h\phi_{h/2}|||, \qquad \widetilde{\mu}_H = \|\varrho^{1/2}(\phi_{h/2} - \Pi_h\phi_{h/2})\|_{L^2(\Gamma)}.$$

over the number $N = \#\mathcal{T}_h$ of elements for uniform and $\widetilde{\mu}_H$-adaptive *anisotropic* mesh-refinement. Throughout we use $\theta = 0.5$ for the marking step (v) of Algorithm 3.3 and $\tau = 0.5$ for the decision which kind of refinement is chosen, c.f. Section 8.1 and Figure 24. Note that our analytical results only provide

$$\widetilde{\mu}_H \le \mu_H \lesssim \eta_H \le \widetilde{\eta}_H \lesssim \sigma(\mathcal{T}_h)^{1/2}\widetilde{\mu}_H,$$

which states equivalence of the error estimators only in case of isotropic mesh-refinement. However, we observe that even for adaptive anisotropic refinement the curves of the error estimators are (up to a certain range) parallel. This gives empirical evidence that the factor $\sigma(\mathcal{T}_h)^{1/2}$ is too pessimistic and can be dropped. Moreover, we have experimental evidence for reliability and efficiency of all error estimators, which is reflected by the boundedness of the experimental saturation constant $q = |||\phi - \phi_{h/2}|||/|||\phi - \phi_h|||$ which satisfies $q \le 0.75$ and $q \le 0.7$ for Problem 7.1 and Problem 7.2, respectively.

We first consider Example 7.1: Figure 26 shows the mesh $\mathcal{T}_h^{(19)}$ with $N = 2846$ elements obtained by $\widetilde{\mu}_H$-adaptive anisotropic mesh-refinement as well as the corresponding discrete solution $\phi_h^{(19)}$. We stress that the implemented algorithm does some additional marking to ensure that $\varrho_j/\varrho_k \le 4$ as well as $h_j/h_k \le 4$ for all neighbouring elements $T_j, T_k \in \mathcal{T}_h^{(\ell)}$. This

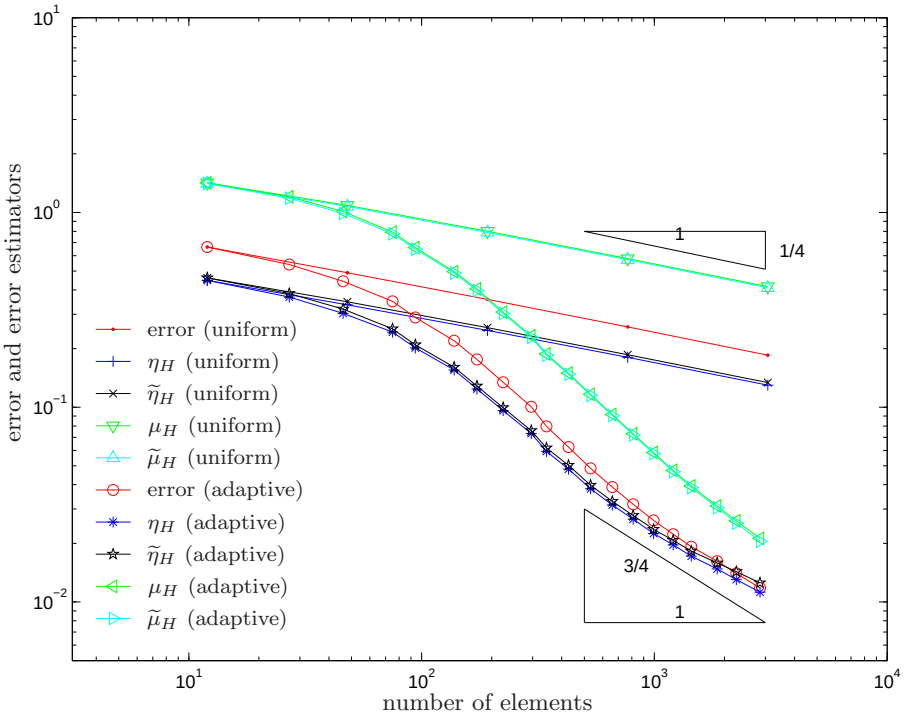

FIGURE 27. Error $|||\phi - \phi_h|||$ and error estimators $\eta_H, \widetilde{\eta}_H, \mu_H, \widetilde{\mu}_H$ in Screen Problem 7.1 for uniform and $\widetilde{\mu}_H$-adaptive anisotropic mesh-refinement, where we chose $\theta = 0$ resp. $\theta = 0.5$ in Algorithm 3.3 for the marking strategy and $\tau = 0.5$ to steer the anisotropic mesh-refinement. A comparison with Figure 19 shows that anisotropic (instead of isotropic) mesh-refinement is necessary (and sufficient) to retain the optimal order of convergence.

explains the refinement towards the reentrant corner at $(1, 1, 0)$ of Γ, where the solution appears to be smooth. The mesh reflects the singularities of ϕ along these edges. As already stated above, uniform mesh-refinement leads to a suboptimal convergence of the error $|||\phi - \phi_h|||$ of order $\mathcal{O}(N^{-1/4})$. The proposed adaptive anisotropic strategy reveals the optimal order of convergence $\mathcal{O}(N^{-3/4})$. Moreover, we observe that for the adaptive strategy η_H tends to the error $|||\phi - \phi_h|||$ in the following sense: Figure 27 shows that the experimental reliability constant $C_{\mathrm{rel}} = |||\phi - \phi_h|||/\eta_H$ tends to 1 with increasing number of elements. On the other hand the influence of the error caused by using the L^2-projection to compute $\widetilde{\eta}_H$ and $\widetilde{\mu}_H$ grows. The deviations increase from $\widetilde{\eta}_H/\eta_H \approx 1.01$ and $\mu_H/\widetilde{\mu}_H \approx 1.04$ for uniform refinement reaching values of approximately $\widetilde{\eta}_H/\eta_H \approx 1.04$ and $\mu_H/\widetilde{\mu}_H \approx 1.12$ for the last step of the adaptive computation.

Finally, we consider the adaptive anisotropic strategy for Example 7.2. Figure 28 shows the adaptively generated mesh $\mathcal{T}_h^{(14)}$ with $N = 4512$ elements. We observe strong anisotropic refinement towards the edges of the cube's surface. This corresponds to the singular behaviour of the corresponding discrete solution $\phi_h^{(14)}$ along the edges. As in the previous example the

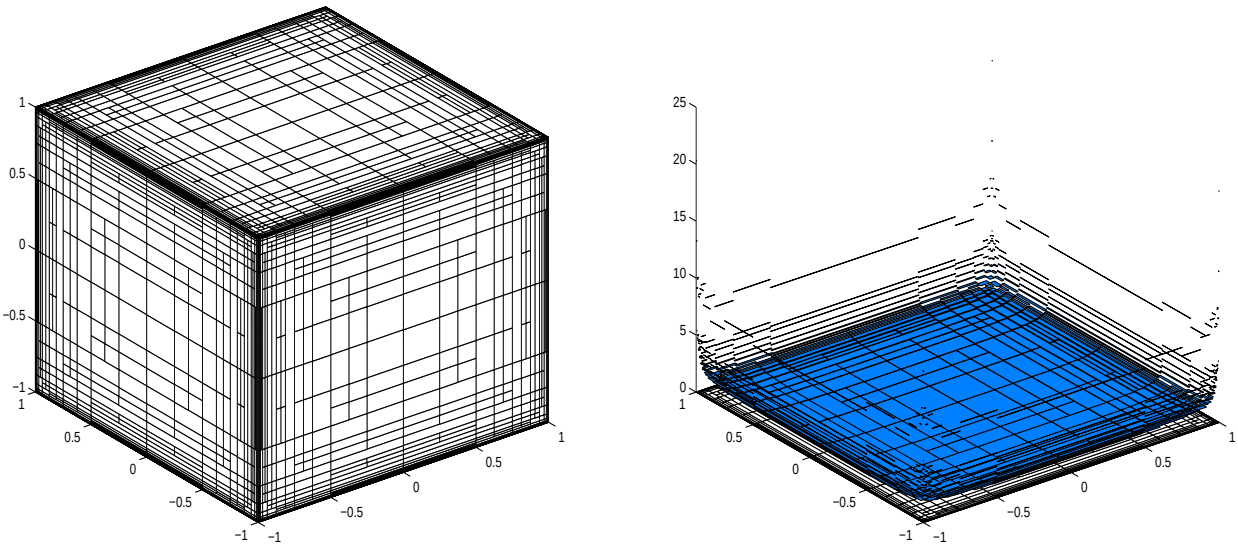

FIGURE 28. Mesh $\mathcal{T}_h^{(14)}$ with $N = 4512$ elements in Capacity Problem 7.2 (left) obtained by $\widetilde{\mu}_H$-adaptive anisotropic mesh-refinement. We used the parameters $\theta = 0.5$ in Algorithm 3.3 for marking and $\tau = 0.5$ to decide the type of refinement, c.f. Section 8.1. The discrete solution $\phi_h^{(14)}$ coincides on each square screen of the cube. We plot $\phi_h^{(14)}$ over the top screen (right), which shows singularities along the edges and at the corners.

optimal convergence order of $\mathcal{O}(N^{-3/4})$ is retrieved by the $\widetilde{\mu}_H$-adaptive anisotropic strategy. Again, we obtain a slight increase of the significance of the approximation error caused by the L^2-projection. The quotients $\widetilde{\eta}_H/\eta_H$ and $\mu_H/\widetilde{\mu}_H$ plotted in Figure 23 increase with the number of elements from $\widetilde{\eta}_H/\eta_H \approx 1.028$ and $\mu_H/\widetilde{\mu}_H \approx 1.06$ for uniform refinement to $\widetilde{\eta}_H/\eta_H \approx 1.034$ and $\mu_H/\widetilde{\mu}_H \approx 1.17$ for adaptive refinement, respectively. Suprisingly and in contrast to all other experiments, the experimental reliability constant does not tend to 1 with increasing number of adaptively generated anisotropic elements. We even observe in Figure 23 that $C_{\rm rel} = |||\phi - \phi_h|||/\eta_H$ can be larger for anisotropic than for uniform mesh-refinement.

9. Conclusions and Remarks

9.1. Analytical Results. In this paper, we derived a posteriori error estimators for the Galerkin boundary element method by use of the well-known h-$h/2$-strategy. For both, the weakly singular integral equation and the hypersingular integral equation, we provided estimators μ_H that are equivalent to the basic error estimator $\eta_H := |||\phi_{h/2} - \phi_h|||$. Here, ϕ_h and $\phi_{h/2}$ are Galerkin solutions with respect to a mesh $\mathcal{T}_h$ and its uniform refinement $\mathcal{T}_{h/2}$. The advantage of the equivalent error estimator μ_H is that the nonlocal energy norm $|||\cdot|||$ is replaced by a weighted L^2- or H^1-seminorm, respectively. Therefore, the local contributions of μ_H are capable to steer an h-adaptive mesh-refinement. There always holds efficiency

$$\mu_H \lesssim \eta_H \le |||\phi - \phi_h||| \tag{9.1}$$

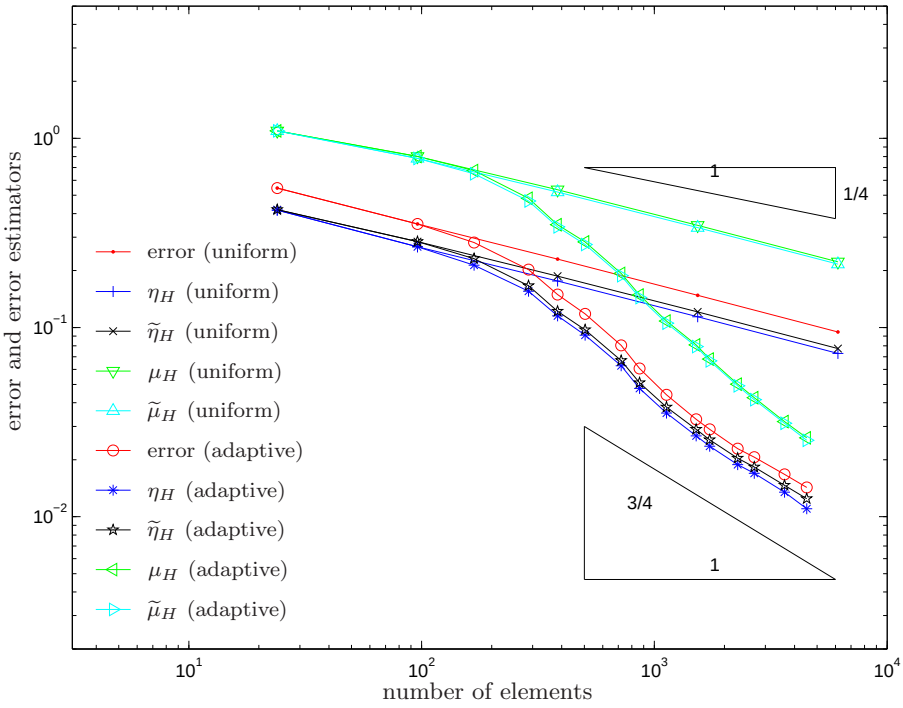

FIGURE 29. Error $|||\phi - \phi_h|||$ and error estimators $\eta_H, \widetilde{\eta}_H, \mu_H, \widetilde{\mu}_H$ in Capacity Problem 7.2 for uniform and $\widetilde{\mu}_H$-adaptive anisotropic mesh-refinement, where we chose $\theta = 0$ resp. $\theta = 0.5$ in Algorithm 3.3 for the marking strategy and $\tau = 0.5$ to steer the anisotropic mesh refinement. A comparison with Figure 22 shows that anisotropic (instead of isotropic) mesh-refinement is necessary (and sufficient) to retain the optimal order of convergence.

under very weak assumptions on the triangulation $\mathcal{T}_h$ used. The converse inequality

$$\eta_H \lesssim \mu_H \tag{9.2}$$

could only be proven for 2D and isotropic mesh-refinement in 3D. More precisely, the constant in this estimate depends on the shape regularity of $\mathcal{T}_h$. First numerical experiments for Symm's integral equation in 3D indicate that this result is too pessimistic in the sense that (9.2) is observed to hold even for anisotropic mesh-refinement. The reliability estimate

$$|||\phi - \phi_h||| \lesssim \eta_H \tag{9.3}$$

depends crucially on the saturation assumption

$$|||\phi - \phi_{h/2}||| \leq q\, |||\phi - \phi_h||| \quad \text{with a uniform constant } q < 1. \tag{9.4}$$

Contrary to the finite element method, the saturation assumption has not been proven for the boundary element method, yet. However, in all numerical experiments, we got empirical evidence that the saturation assumption holds. This might be due to additional regularity of the exact solution. For Symm's integral equation, for instance, all exact solutions appeared to belong not only to the energy space $\widetilde{H}^{-1/2}(\Gamma)$ but also at least to $H^{-\varepsilon}(\Gamma)$, for all $\varepsilon > 0$.

9.2. Advantages of the Proposed Method. Usually, other a posteriori error estimators involve the evaluation of the residual, e.g. [F1, F2, CMS, CMPS], or higher-order elements, e.g. [CP2, CP3, FFP], and thus need additional implementation. One great advantage of the proposed error estimators is that there is almost no implementational overhead. First, the error estimator η_H is simply computed by the Galerkin orthogonality

$$\eta_H^2 = |||\phi_{h/2} - \phi_h|||^2 = |||\phi_{h/2}|||^2 - |||\phi_h|||^2, \tag{9.5}$$

where both discrete energies are byproducts of the computation: The coefficient vector $\mathbf{x} \in \mathbb{R}^N$ of ϕ_h solves the Galerkin system $\mathbf{Ax} = \mathbf{b}$, so that the corresponding energy reads $|||\phi_h|||^2 = \mathbf{x} \cdot \mathbf{Ax} = \mathbf{x} \cdot \mathbf{b}$.

Second, the implementation of a mesh-size weighted L^2- or H^1-seminorm for piecewise polynomials is fairly standard and can be performed analytically without any additional quadrature errors. Contrary to that, residual-based error estimators usually involve certain quadrature rules to integrate the residual. These quadrature formulae have to deal, by others, with weak singularities according to the integral operators V and W.

With respect to the error estimation, we stress that the efficiency estimate for η_H holds with *known* constant $C_{\text{eff}} = 1$ so that η_H gives a concrete lower bound for the unknown error $|||\phi - \phi_h|||$. In the numerical experiments, we observed that the error estimation of η_H is very accurate. The accuracy of η_H is even improved if the mesh $\mathcal{T}_h$ is adaptively generated by the introduced adaptive algorithm. We thus propose to use μ_H to steer the adaptive mesh-refinement and to use η_H for the simultaneous error control.

9.3. Obvious Extensions of the Analysis. Instead of the h-$h/2$-strategy, one can even think of a posteriori error estimators arising from a p-$(p+1)$-strategy: In case of Symm's integral equation with lowest-order boundary elements, let $\phi_{h,0} \in \mathcal{P}^0(\mathcal{T}_h)$ and $\phi_{h,1} \in \mathcal{P}^1(\mathcal{T}_h)$ be Galerkin solutions corresponding to a given triangulation $\mathcal{T}_h = \{T_1, \dots, T_N\}$. As for the h-$h/2$-strategy, we have nestedness of the discrete spaces $\mathcal{P}^0(\mathcal{T}_h) \subseteq \mathcal{P}^1(\mathcal{T}_h)$ which yields

$$|||\phi - \phi_{h,0}|||^2 = |||\phi - \phi_{h,1}|||^2 + |||\phi_{h,1} - \phi_{h,0}|||^2. \tag{9.6}$$

From this, we infer efficiency of the error estimator

$$\eta_P := |||\phi_{h,1} - \phi_{h,0}||| \le |||\phi - \phi_{h,0}|||. \tag{9.7}$$

As above, the saturation assumption

$$|||\phi - \phi_{h,1}||| \le q\,|||\phi - \phi_{h,0}||| \quad \text{with a uniform constant } q < 1, \tag{9.8}$$

provides reliability

$$|||\phi - \phi_{h,0}||| \le \frac{1}{\sqrt{1-q^2}}\,\eta_P. \tag{9.9}$$

Now, the same techniques as for η_H apply to prove that the ϱ-weighted error estimator

$$\mu_P := \|\varrho^{1/2}(\phi_{h,1} - \phi_{h,0})\|_{L^2(\Gamma)} \tag{9.10}$$

satisfies $\mu_P \lesssim \eta_P \lesssim \mu_P$, where only the upper estimate depends on the shape regularity of $\mathcal{T}_h$. Numerical experiments and a comparison of the corresponding adaptive strategies are postponed to a forthcoming paper.

Acknowledgement. The results of this paper have been presented on the conference *BETA 2007 – Boundary Elements: Theory and Applications*, which took place in May 2007 in Hannover on the occasion of Professor Ernst Stephan's 60^{th} birthday.

References

[CMPS] C. Carstensen, M. Maischak, D. Praetorius, E. Stephan: *Residual-based a posteriori error estimate for hypersingular equation on surfaces*, Numer. Math. 97 (2004), 397–425.

[CMS] C. Carstensen, M. Maischak, E. Stephan: *A posteriori estimate and h-adaptive algorithm on surfaces for Symm's integral equation*, Numer. Math. 90 (2001), 197–213.

[CP1] C. Carstensen, D. Praetorius: *A Posteriori error control in adaptive qualocation Boundary element analysis for a logarithmic-kernel integral equation of the first kind*, SIAM J.Sci.Comp. 25 (2004), 259-283.

[CP2] C. Carstensen, D. Praetorius: *Averaging techniques for the effective numerical solution of Symm's integral equation of the first kind*, SIAM J.Sci.Comp. 27 (2006), 1226–1260.

[CP3] C. Carstensen, D. Praetorius: *Averaging Techniques for the A Posteriori BEM Error Control for a Hypersingular Integral Equation in Two Dimensions*, SIAM J.Sci.Comp. 29 (2007), 782–810.

[ChS] G.A. Chandler, I.H. Sloan: *Spline qualocation methods for boundary integral equations.* Numer. Math. 58 (1990), 537-567.

[CS] M. Costabel, E. Stephan: *A direct boundary integral equation method for transmission problems.* J. Math. Anal. Appl., 106 (1985), 2, 367–413.

[D] W. Doerfler: *A convergent adaptive algorithm for Poisson's equation*, SIAM J.Numer.Anal. 33 (1996), 1106–1124.

[DN] W. Doerfler, R. Nochetto: *Small data oscillation implies the saturation assumption*, Numer. Math. 91 (2002), 1–12.

[F1] B. Faermann. *Localization of the Aronszajn-Slobodeckij norm and application to adaptive boundary element methods. Part I. The two-dimensional case.* IMA J. Numer. Anal. 20 (2000), 203-234.

[F2] B. Faermann. *Localization of the Aronszajn-Slobodeckij norm and application to adaptive boundary element methods. Part II. The three-dimensional case.* Numer. Math. 92 (2002), 467-499.

[GHS] I.G. Graham, W. Hackbusch, S.A. Sauter: *Finite elements on degenerate meshes: Inverse-type inequalities and applications*, IMA J. Numer. Anal. 25 (2005), 379–407.

[FFP] S. Ferraz-Leite, S. Funken, D. Praetorius: *Averaging on large patches for integral equations in 3D*, work in progress 2007.

[M] M. Maischak: *The Analytical Computation of the Galerkin Elements for the Laplace, Lamé and Helmholtz Equation: 2D BEM*, Preprint (1999), *3D BEM*, Preprint (2000), Institut für Angewandte Mathematik, Universität Hannover.

[McL] W. McLean: *Strongly elliptic systems and boundary integral equations.* Cambridge University Press, Cambridge 2000.

[SZ] L. Scott, S. Zhang: *Finite Element Interpolation of Nonsmooth Functions Satisfying Boundary Conditions*, Math. Comp. 54 (1990)

Institute for Analysis and Scientific Computing, Vienna University of Technology, Wiedner Hauptstrasse 8-10, A-1040 Vienna, Austria

Correspondence to: `Dirk.Praetorius@tuwien.ac.at`